A ROE SOLVER FOR A MULTI-CLASS TRAFFIC FLOW MODEL

by

Reanne Bowlby

B.A. (Mathematics), Western Washington University, 2007

A Thesis submitted in partial fulfillment
of the requirements for the degree of
Master of Science
in the
Department of Mathematics
Faculty of Science

SIMON FRASER UNIVERSITY
Fall 2011

APPROVAL

Name:	Reanne Bowlby
Degree:	Master of Science
Title of Thesis:	A Roe Solver for a Multi-Class Traffic Flow Model
Examining Committee:	Dr. Steve Ruuth (Chair)
	Dr. John Stockie, Professor, Mathematics Simon Fraser University (Senior Supervisor)
	Dr. David J. Muraki, Professor, Mathematics Simon Fraser University (Supervisor)
	Dr. JF Williams, Professor, Mathematics Simon Fraser University (Examiner)
Date Approved:	December 1, 2011

Declaration of
Partial Copyright Licence

Abstract

The dynamics of traffic flow, where drivers are distinguished by distinct velocity classes, can be described using a nonlinear system of hyperbolic conservation laws. The equations are a generalization of the scalar Lighthill, Whitham and Richards (LWR) model. We first derive the exact solution to the corresponding Riemann problem in the case of two classes. We then motivate the use of a Roe solver and derive the Roe linearization with a corresponding entropy fix. Finally, we implement the scheme for two- and three-class flow using CLAWPACK, a publicly available package for solving hyperbolic conservation laws.

For my family.

"To see is to see a better way; to perceive any problem clearly is to begin to create its solution. All we need is the wisdom and patience to keep looking and the love to hold what we see up to the light of understanding."

— Laurence Boldt

Acknowledgments

I would like to thank my senior supervisor John Stockie for starting me down this journey and for patiently guiding my development as a mathematician. I greatly appreciate your commitment throughout my degree and especially for your insights during the revisions of this thesis. I would also like to thank my supervisor Dave Muraki for teaching me what it means to truly communicate ideas. Our discussions challenged me to reach a deeper level of understanding and mathematical reasoning that will be an asset to me throughout my life. And finally, a special thanks to my family and friends for supporting me and believing in me through this process.

Contents

List of Figures

Chapter 1

Introduction

Lighthill and Whitham (1955) [17] and Richards (1956) [20] independently proposed a continuum model to describe traffic flow known as the LWR model. It describes the evolution of the density of traffic ρ along a one-dimensional road using the conservation equation,

$$\rho_t + (\rho v(\rho))_x = 0, \tag{1.1}$$

where v is a given function of the density chosen to best represent empirical data. Known for its simplicity, the LWR model does a remarkable job of capturing real traffic phenomenon such as shock waves and anisotropic behavior which is the tendency for drivers to react only to the vehicles ahead [21]. However, there are other observed traffic patterns that this model cannot predict.

Many extensions of the LWR model have been developed in an attempt to explain more complex traffic patterns. Recently, much attention has been given to developing a model that accounts for a heterogeneous population of drivers. These different classes of drivers can include different desired maximum velocities [25, 29, 28, 3, 26, 19], multiple lanes [30, 31], or varying vehicle length [2, 3].

Wong and Wong [25] were one of the first to formulate a multi-class extension of the LWR model to account for multiple driver types. Their paper characterized a driver's class in terms of a desired maximum velocity. A first order Lax-Friedrichs scheme was used to solve a system with nine classes of vehicles that was then compared against actual traffic data. Interestingly, this multi-class system was able to describe some of the more complex traffic patterns that the LWR model could not. One such result was able to replicate platoon dispersion which is the tendency for drivers that are grouped together to

disperse. The following year, a second paper was produced [28] with the same model, but with a more accurate numerical scheme: a fifth order weighted essentially non-oscillatory scheme (WENO). It was found that the Lax-Friedrichs scheme was so diffusive that it had smoothed out an interesting staircase like behavior captured by the WENO scheme. Because of its accuracy, WENO has been used in other traffic flow models such as in [29] where an alternative velocity function is studied for three-class traffic flow.

Around the same time, Benzoni-Gavage and Colombo [3] developed a model for a population of n driver classes. Their work focused on the analytical solution to the Riemann problem and worked out a particular example of the exact solution for $n = 2$ classes. Part of the motivation for this work was to provide the analytical solution needed for a Godunov-type numerical scheme.

We would like to mention that there are many other multi-class traffic models that are not extensions of the LWR equation [12, 4]. One such traffic model was developed by Hoogendoorn and Bovy [12] to account for the fact that drivers slow down gradually unlike in the LWR model where velocities change instantaneously. To produce this type of behavior the gas-kinetic equations, not discussed in this thesis, were used as a basis and were then extended to allow for different classes of drivers each seeking to drive at a class-desired velocity. It was demonstrated that these two processes, gradually slowing down due to other vehicles and seeking a desired maximum velocity, can produce localized structures seen in actual traffic.

While there has been a lot of interest on developing multi-class models, relatively little has been done on testing different numerical schemes. The purpose of this thesis is to derive a Riemann solver, particularly a Roe solver, for a system of hyperbolic conservation laws corresponding to multi-class traffic flow. The equations are of LWR type with a different maximum velocity characterizing each class. Employing a numerical scheme that builds in knowledge of the exact solution will produce equivalent and in some cases improve on the accuracy of the WENO approach. Furthermore, through the use of CLAWPACK, a publicly available tool for solving hyperbolic PDEs using Riemann solvers, the implementation of this scheme is made relatively easy.

In chapter 2, background information is provided about 1-dimensional scalar traffic flow, including discussion of the LWR model and the fundamental diagram for traffic. We also discuss the idea behind the Riemann problem and the method of characteristics. In chapter 3 we introduce finite volume methods, particularly Godunov's method and Roe's

method, for scalar conservation laws. Chapter 4 provides a detailed analytical solution to the Riemann problem for two-class traffic flow. And finally chapter 5 describes the numerical implementation of a Roe solver for two-class traffic flow. Comparisons of two-, three- and nine-class results are made with two different WENO schemes from [28, 29]. This work sets the stage for further research on multi-class traffic flow.

Chapter 2

Scalar Conservation Laws

Imagine an infinitely long, straight tunnel with no entrances or exits, filled with vehicles. In this tunnel vehicles are characterized by their density (ρ), velocity (v) and flow rate (f) also referred to as flux. Assuming that motion is only in the direction x, we can take ρ, v and f to be functions of x and t. The flow rate, also referred to as flux, is written $f = v(\rho)\rho$ where the velocity function $v(\rho)$ is typically chosen based on empirical data. Any model for such a scenario should at least conserve vehicles.

2.1 Conservation Laws

Conservation of vehicles means that the change in density along a small stretch of tunnel from (x_1, x_2) is equal to the flux through x_1 i.e. $f(\rho(x_1, t))$ minus the flux through x_2 i.e. $f(\rho(x_2, t))$,

$$\frac{d}{dt}\int_{x_1}^{x_2} \rho(x,t)dx = f(\rho(x_1,t)) - f(\rho(x_2,t)). \tag{2.1}$$

As the segment (x_1, x_2) shrinks to a point, equation (2.1) becomes the differential conservation law:

$$\frac{\partial}{\partial t}\rho(x,t) + \frac{\partial}{\partial x}f(\rho(x,t)) = 0, \quad \text{where} \quad \rho(x,0) = g(x) \tag{2.2}$$

and $g(x)$ is the initial density. Equation (2.2) can be written in non-conservative form by expanding the partial derivative of f and assuming that f and ρ are smooth functions of x. This yields:

$$\frac{\partial}{\partial t}\rho(x,t) + f'(\rho(x,t))\frac{\partial}{\partial x}\rho(x,t) = 0. \tag{2.3}$$

This gives an evolution equation for the density, assuming the flux function is known. In some models such as the shallow water equations, the flux is determined by a second PDE derived from the conservation of momentum. Models with a separate PDE for the velocity function have been developed for traffic flow problems which account for a driver's reaction time (i.e. acceleration) [21]. Another option is to use empirical data which shows a strong correlation between the flux and density.

Many flux functions have been proposed for traffic flow, the simplest being the Greenshield's flux where

$$v(\rho) = \alpha(1 - \frac{\rho}{\rho_m}) \tag{2.4}$$

and

$$f(\rho) = \alpha\rho(1 - \frac{\rho}{\rho_m}). \tag{2.5}$$

These equations imply that there is no flow when the density is at its maximum $\rho = \rho_m$ or minimum $\rho = 0$, and that the highest flux will be achieved when when density is at half the maximum value. The parameter α is the maximum velocity that a vehicle can reach, the speed limit.

The conservation law (2.2) and equation (2.5) were proposed as a model of traffic flow by Lighthill, Whitham and independently by Richards. From hereon it will be referred to as the LWR model. Without loss of generality we use a scaled flux function such that $\alpha = \rho_m = 1$. We remark that the chosen flux function is convex, since $f'' = \frac{-2\alpha}{\rho_m}$ is strictly negative. Our analytical and numerical methods will rely on this fact.

2.2 Method of Characteristics

We now turn to a common technique for solving a conservation law with convex flux. The method of characteristics capitalizes on the fact that it is possible to find curves $X(t)$ in the xt-plane, along which the solution $\rho(X(t), t) = \rho_0$ is constant. Assume there exists such a curve $X(t)$ along which the solution is constant such that

$$\frac{d}{dt}\rho(X(t), t) = 0. \tag{2.6}$$

Expanding (2.6) gives,

$$\frac{d}{dt}\rho(X(t), t) = \rho_t + \frac{dX}{dt}\rho_x = 0. \tag{2.7}$$

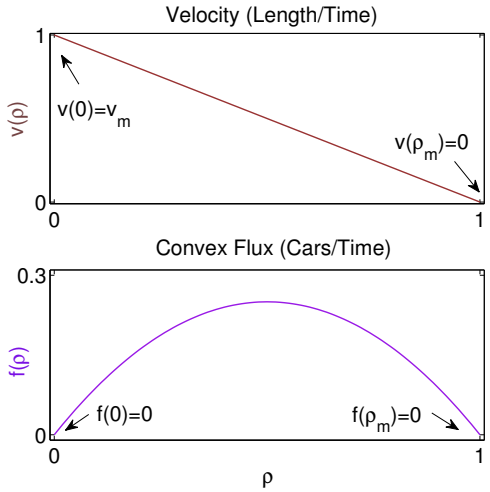

Figure 2.1: The velocity and flux functions for the LWR model

This is exactly equation (2.3) when

$$\frac{dX}{dt} = f'(\rho(X(t),t)) = f'(\rho_0). \tag{2.8}$$

Curves of constant density are found by solving this ODE for $X(t)$:

$$X(t) = f'(\rho_0)t + c. \tag{2.9}$$

These curves of constant ρ are called characteristic curves and for scalar conservation laws these characteristics are straight lines with slope $\frac{1}{f'(\rho_0)}$ in the xt-plane. The slope of a characteristic is called the characteristic speed. Finally, the value of ρ_0 along each characteristic is found by tracing along the characteristic back to the initial value $\rho(x,0) = g(x)$.

For a linear conservation law this information would be enough to determine the solution for all x and t because characteristics are parallel and therefore fill the entire xt-plane. However, for nonlinear conservation laws, since characteristics are not always parallel, we must understand how to deal with the two scenarios where characteristics collide and where they diverge. The idea of convexity is important here because it implies that the characteristic speed $f'(\rho)$ is varying monotonically as ρ varies. Without convex flux more complicated solutions can arise in which a combination of both colliding and diverging characteristics can occur [16]. To simplify our analysis we study the Riemann problem which is a simplified initial condition consisting of piecewise constants.

2.3 Riemann Problem

A Riemann problem is a conservation law (2.2) paired with piecewise constant initial data

$$\rho(x,0) = \begin{cases} \rho_L & \text{if } x \leq 0, \\ \rho_R & \text{if } x > 0. \end{cases}$$

Studying the Riemann problem allows us to focus on the case when characteristics collide and when they diverge. First, let's discuss what happens when characteristics collide.

2.3.1 Case 1: $f'(\rho_L) > f'(\rho_R)$, Characteristics Collide

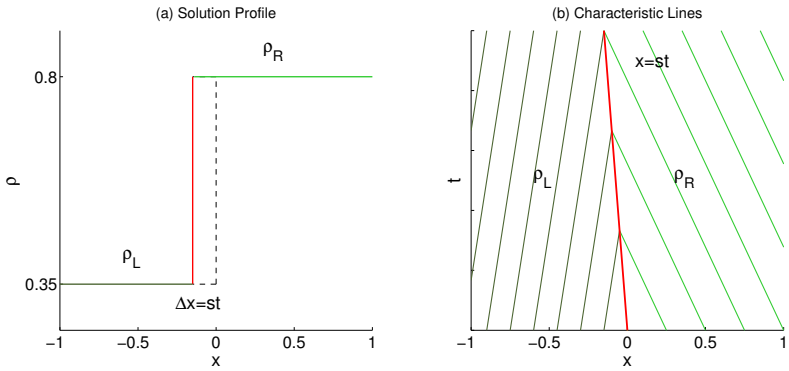

Figure 2.2: The solution profile is given for the LWR model where $f'(\rho_L) > f'(\rho_R)$. In plot (a) the dashed black line is the initial condition. The red line shows the discontinuity propagating backward in time. For $f'(\rho_L) > f'(\rho_R)$ to occur in traffic flow the density must be lower on the left implying that velocity on the left is greater. If traffic on the left is moving faster then it will catch up to the slower moving traffic causing a shock. Figure (b) shows how the characteristics in the xt-plane collide to form a shock.

The characteristics will be curves $X(t) = f'(\rho)t + x_0$. The green characteristics in Figure 2.2 are lines along which the density is ρ_L or ρ_R, with slopes given respectively by:

$$f'(\rho_L) = 1 - 2\rho_L \tag{2.10}$$

$$f'(\rho_R) = 1 - 2\rho_R \tag{2.11}$$

Notice that the slopes in the figure are actually $\frac{1}{f'}$ because t is on the vertical axis. Since $f'(\rho_L) > f'(\rho_R)$, characteristics will collide creating what is known as a shock wave, characterized by a jump in the density. This discontinuity in the density propagates with speed

s given by the Rankine Hugoniot condition or RHC,

$$s = \frac{f(\rho_L) - f(\rho_R)}{\rho_L - \rho_R}.$$

The shock speed for the LWR model is then $s = 1 - \rho_L - \rho_R$. Details of the derivation of the RHC can be found in [11]. Notice that a shock does not mean that vehicles collide, but rather their speed changes instantaneously to that of the speed of the ρ_R traffic to avoid collision.

One more condition is needed in order to ensure the solution is unique. This condition is chosen to put a restraint on how the entropy of the system behaves. The most common entropy condition is the Lax-entropy condition which requires the shock speed to lie between the two characteristic speeds. This idea is written as

$$f'(\rho_L) > s > f'(\rho_R). \tag{2.12}$$

The solution to the Riemann problem is then given by,

$$\rho(x,t) = \begin{cases} \rho_L & \text{if } x \leq st, \\ \rho_R & \text{if } x > st. \end{cases} \tag{2.13}$$

2.3.2 Case 2: $f'(\rho_L) < f'(\rho_R)$, Characteristics Diverge

In case 2, characteristics diverge from each other thereby creating a gap between the two green characteristics $x = f'(\rho_L)t$ and $x = f'(\rho_R)t$ shown in Figure 2.3. To determine how the density varies between these two characteristics we will use what is called the similarity solution, details for which are given in [15]. Since characteristics must be straight lines, and uniqueness requires that characteristics cannot cross, this suggests that we look for a solution of the form $\rho(x,t) = w(\frac{x}{t})$ in the wedge between the leading and tailing characteristics. Substituting this into the conservation law we find that $f'(w) = \frac{x}{t}$ or $w = (f')^{-1}(\frac{x}{t})$. Thus, characteristics in this intermediate state have slope $\frac{x}{t}$, creating a fan in the xt-plane corresponding to the density spreading out. This is called a rarefaction wave. For the LWR model the constant density given by the characteristics in the expansion fan is $w(\frac{x}{t}) = \frac{1}{2} - \frac{x}{2t}$. The full solution to the rarefaction case can then be written as

$$\rho(x,t) = \begin{cases} \rho_L & \text{if } x < f'(\rho_L)t, \\ w(\frac{x}{t}) & \text{if } f'(\rho_L)t \leq x \leq f'(\rho_R)t, \\ \rho_R & \text{if } x > f'(\rho_R)t. \end{cases} \tag{2.14}$$

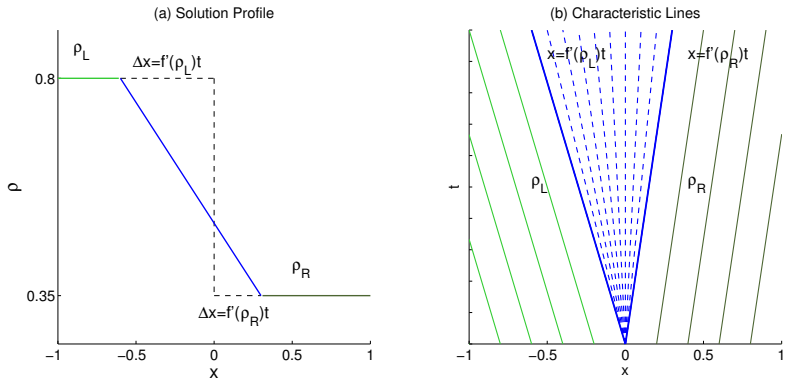

Figure 2.3: Figure (a) shows the solution profile for a rarefaction. The dashed black line is the initial condition. The blue line shows the rarefaction wave spreading out in time. For $f'(\rho_L) < f'(\rho_R)$ to occur in traffic flow, density must be higher on the left, implying that the velocity on the left is slower. If cars on the left are moving slower then they will get further away from the leading cars creating a spreading out effect. Plot (b) shows the characteristics diverging to form a rarefaction wave.

Chapter 3

Numerics for Scalar Conservation Laws

We now discuss numerical methods for scalar hyperbolic conservation laws. In particular this section will give an overview of finite volume methods as well as a first glimpse of the Roe scheme, a particular type of finite volume method, which will lead to our main work in chapter 5.

Hyperbolic conservation laws require a special choice of numerical method for two reasons. First, traditional finite difference approximations break down near discontinuities by failing to capture the correct shock speeds. And second, since the equation for our model is conservative, it makes sense to require the numerical method to also be conservative. It turns out that a non-conservative scheme will not converge for discontinuous solutions [24]. Because of these requirements finite volume methods are used which derive the discrete equations based on an alternate formulation of the PDE called the integral form.

The integral form of a conservation law is useful for two reasons. First, conservation laws are derived from physical conservation principles that can be expressed as integral relations on control volumes. And second, the integral form of a conservation law allows for the possibility of discontinuous solutions [15].

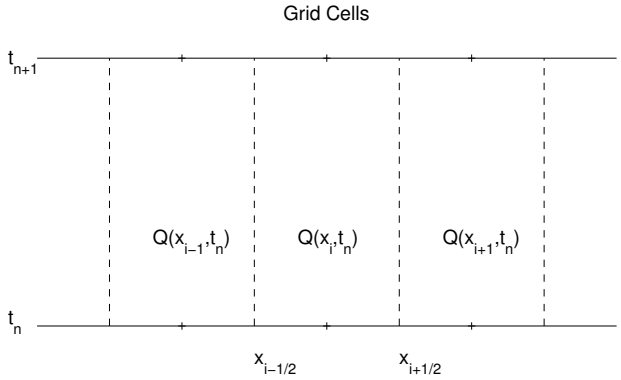

Figure 3.1: A grid cell is a rectangular box in the xt-plane over which the conservation law is being integrated.

3.1 Finite Volume Methods

Let us begin by understanding the integral form of the following scalar conservation law,

$$\rho_t + f(\rho)_x = 0. \tag{3.1}$$

We will integrate (3.1) over a finite volume in the xt-plane called a grid cell shown in Figure 3.1. The cell is defined in the x direction by the left cell edge at $x_{i-1/2}$ and the right cell edge by $x_{i+1/2}$ and in the t direction from t^n to t^{n+1}. Integrating over this control volume first in space and then in time yields,

$$\int_{x_{i-1/2}}^{x_{i+1/2}} \rho(x, t_{n+1})\, \mathrm{d}x = \int_{x_{i-1/2}}^{x_{i+1/2}} \rho(x, t_n)\, \mathrm{d}x - \int_{t_n}^{t_{n+1}} f(\rho(x_{i+1/2}, t))\, \mathrm{d}t + \int_{t_n}^{t_{n+1}} f(\rho(x_{i-1/2}, t))\, \mathrm{d}t. \tag{3.2}$$

Equation (3.2) is the integral form for the conservation law (3.1). In words, it states that the total number density in a cell at time t_{n+1} is equal to the total number density in the cell at t_n plus the incoming density minus the outgoing density. The integral form is an exact representation of the conservation law and is the foundation for a conservative numerical scheme.

We define Q_i^n to be an approximation of the average density in a cell:

$$Q_i^n \approx \frac{1}{\Delta x} \int_{x_{i-1/2}}^{x_{i+1/2}} \rho(x, t_n)\, \mathrm{d}x \tag{3.3}$$

and $F^n_{i-1/2}$ as the numerical flux, which is an approximation to the average flux across a cell interface:

$$F^n_{i-1/2} \approx \frac{1}{\Delta t}\int_{t_n}^{t_{n+1}} f(\rho(x_{i-1/2}, t))\ \mathrm{d}t. \tag{3.4}$$

A conservative scheme for the scalar conservation law (3.1) is then a numerical method of the form

$$Q^{n+1}_i = Q^n_i + \frac{\Delta t}{\Delta x}\left(F^n_{i-1/2} - F^n_{i+1/2}\right). \tag{3.5}$$

The general idea of finite volume methods is as follows. The domain is broken into cells $i = 1, ..., N$ and Q^n_i denotes the average density in the i^{th} cell. As a result, the solution is approximated by a piecewise constant function as pictured in Figure 3.2. At each cell interface is a local Riemann problem with left state Q^n_{i-1} and right state Q^n_i that can be solved using the method of characteristics discussed in the previous chapter. The beauty of these local Riemann problems is that the flux is constant along each cell interface making integral (3.4) easy to compute.

The following two sections will highlight two closely-related finite volume methods: Godunov's method and Roe's method. They differ in how they derive the numerical flux (3.4). Godunov's method utilizes the exact solution to the Riemann problem, while Roe's method utilizes the solution to an approximate Riemann problem.

3.2 Godunov's Method

As stated above, Godunov's method uses the exact solution to the Riemann problem to determine the density along the cell interface and thereby determining the numerical flux. We define $Q_{i-1/2}$ to be the density along the cell interface $x_{i-1/2}$ obtained by solving the local Riemann problem. If the characteristics emanating from the cell interface between Q_{i-1} and Q_i are all right-going then $Q_{i-1/2} = Q_{i-1}$. If the characteristics are all left-going then $Q_{i-1/2} = Q_i$. From equation (3.4), the numerical flux is simply,

$$F^n_{i-1/2} = f(Q_{i-1/2}). \tag{3.6}$$

In the case where the trailing speed $f'(Q_{i-1}) < 0$ and the leading speed $f'(Q_i) > 0$, which we will call a transonic rarefaction, as shown in red in Figure 3.2, the density along the cell interface is still constant. This is because the cell interface is itself a characteristic line, the particular one with zero speed. Thus, $Q_{i-1/2} = Q_S$ is determined by solving $f'(Q_S) = 0$,

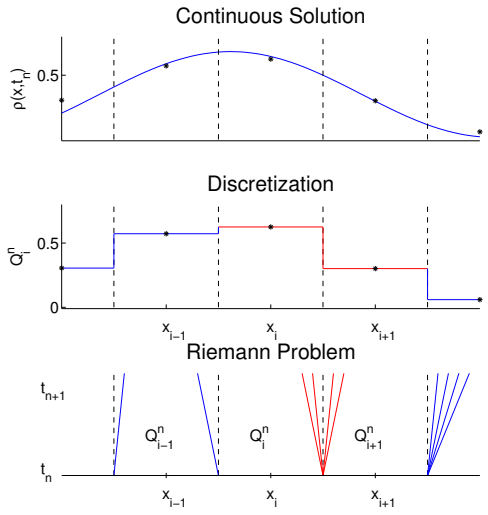

Figure 3.2: The discretization process for finite volume methods is shown in plots 1 and 2. The second figure shows the local Riemann problems that arise at cell interfaces. And the third figure shows the characteristics from equation (3.1) in each grid cell.

where Q_S is the sonic value. Finally, the numerical flux in the case of a transonic rarefaction is

$$F^n_{i-1/2} = f(Q_S). \tag{3.7}$$

A simple rule can be written to determine $F^n_{i-1/2}$ for all possible scenarios of the Riemann problem. If the waves are all right-going then $F^n_{i-1/2} = f(Q_L)$, if the waves are all left-going then $F^n_{i-1/2} = f(Q_R)$ and if the waves are transonic then $F^n_{i-1/2} = f(Q_S)$.

We now have enough information to write a Godunov scheme for a scalar conservation law. The benefit of using this method is that exact information is being incorporated into the numerical scheme. The downside however is that it can be computationally expensive to find the exact solution to the Riemann problem for nonlinear systems of PDEs. For this reason we will discuss a modification of Godunov's method where $F^n_{i-1/2}$ is determined by solving an approximate Riemann problem.

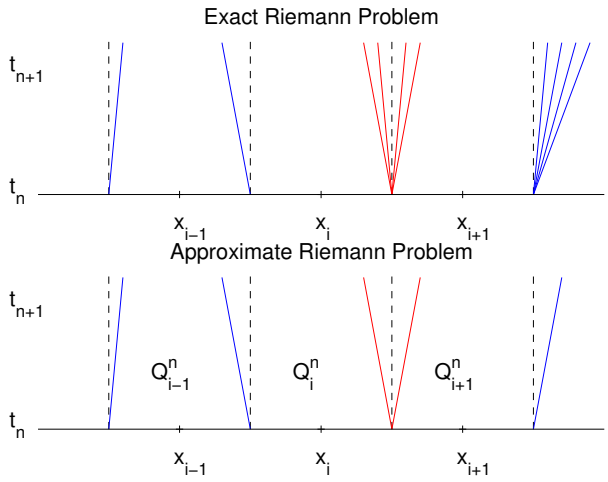

Figure 3.3: Roe's method replaces all non-transonic rarefaction waves with a single wave with the same direction. Transonic rarefactions as shown in red, are replaced with two waves traveling at the leading and trailing speeds of the original rarefaction.

3.3 Roe's Method

Roe's method for scalar conservation laws is nearly identical to Godunov's in terms of the numerical flux. We discuss Roe's method in this chapter however, because it is much easier to visualize and to compare the two methods. Keep in mind that we will extend these ideas to systems where Roe's method will make it considerably less expensive to compute the numerical flux.

The basis for Roe's method is to solve an approximate linearized Riemann problem in which all non-transonic rarefaction waves in the original problem are approximated with a single shock wave traveling in the same direction as the original wave. This is demonstrated by the blue characteristics in Figure 3.3. Approximating a transonic rarefaction with a single wave will not be good enough because the value of the density along the cell interface is neither Q_{i-1} nor Q_i, but some value in between. In this case the transonic rarefaction, as shown in red, must be replaced with two waves traveling at the same speeds as the leading and trailing characteristics of the original rarefaction fan. The sonic value Q_S is a constant state in between the two waves. The discussion of this special case is reserved for the next section.

Deriving a Roe solver relies on finding a linear PDE that approximates equation (3.1) and on deriving the corresponding numerical flux that is consistent with equation (3.4). To approximate a nonlinear PDE with a linear one we must find a constant A such that $f'(\rho) \approx A$ where A depends only on Q_{i-1} and Q_i. Thus, the original nonlinear conservation law

$$\rho_t + f'(\rho)\rho_x = 0 \tag{3.8}$$

is replaced with the linear PDE given by

$$\tilde{\rho}_t + A(Q_{i-1}, Q_i)\tilde{\rho}_x = 0. \tag{3.9}$$

The variable $\tilde{\rho}$ represents the solution to the linear PDE. Roe proposed two criteria for determining A:

1. $A(Q_{i-1}, Q_i) \to f'(v)$ as Q_{i-1} and $Q_i \to v$, a consistency condition for smooth flow.
2. $A(Q_{i-1} - Q_i) = f(Q_{i-1}) - f(Q_i)$ enforcing consistency for shocks.

A more general set of criteria for systems will be given in chapter 5. For the scalar case, A is uniquely determined by condition 2, the Rankine Hugoniot condition for the shock speed

$$A = s = \frac{f(Q_{i-1}) - f(Q_i)}{Q_{i-1} - Q_i}. \tag{3.10}$$

Consider the meaning of replacing $f'(\rho)$ with equation (3.10). It simply states that shocks are left unchanged and all rarefactions are replaced with a single wave propagating at a speed in between the leading and trailing characteristic speeds. For the scalar case this means that Godunov's method and Roe's method are equivalent granted the local Riemann problem does not produce a transonic rarefaction.

Now that we know the linear PDE that is to be solved at each cell interface, we must discuss how we will derive the numerical flux from this approximate Riemann problem to be consistent with the original nonlinear problem. In order to derive the numerical flux for Roe's method we will first derive a general property for the flux across a cell interface.

Flux Property

Consider a single Riemann problem where the domain $D = [-M, M] \times [0, T]$ is large enough to include the shock or rarefaction characteristics emanating from the initial discontinuity. This is illustrated in Figure 3.4. Then let $C_L = \min(s, f'(\rho_L), f'(\rho_R))$ be the slowest wave

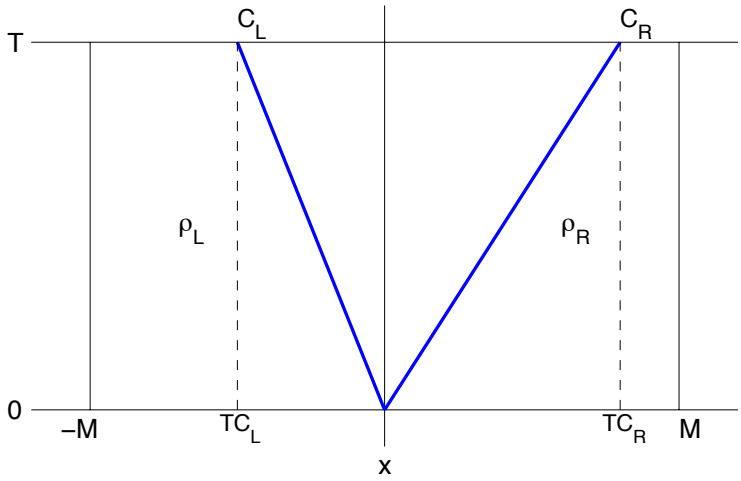

Figure 3.4: The control volume $[-M, M] \times [0, T]$ where M and T are chosen so that the slowest wave speed C_L and fastest wave speed C_R are fully contained in the domain.

speed and $C_R = \max(s, f'(\rho_L), f'(\rho_R))$ be the fastest wave speed . Note that if a shock occurs $C_L = C_R$. Using D and the integral form of our conservation law, we will derive a property that must hold for the flux across a cell interface. This will help us derive a consistent numerical flux for Roe's method. The integral form of the conservation law (3.1) on this control volume reads,

$$\int_{-M}^{M} \rho(x,T)\,\mathrm{d}x = \int_{-M}^{M} \rho(x,0)\,\mathrm{d}x - \int_{0}^{T} f(\rho(M,t))\,\mathrm{d}t + \int_{0}^{T} f(\rho(-M,t))\,\mathrm{d}t. \tag{3.11}$$

Evaluating the right-hand side of this expression yields,

$$\int_{-M}^{M} \rho(x,T)\,\mathrm{d}x = M(\rho_R + \rho_L) + T(f(\rho_L) - f(\rho_R)). \tag{3.12}$$

Now we split the integral on the left-hand side of (3.12) into three integrals as

$$\int_{-M}^{M} \rho(x,T)\,\mathrm{d}x = \int_{-M}^{TC_L} \rho(x,T)\,\mathrm{d}x + \int_{TC_L}^{TC_R} \rho(x,T)\,\mathrm{d}x + \int_{TC_R}^{M} \rho(x,T)\,\mathrm{d}x. \tag{3.13}$$

Two of these three integrals can easily be evaluated leading to

$$\int_{-M}^{M} \rho(x,T)\,\mathrm{d}x = \rho_L(TC_L + M) + \int_{TC_L}^{TC_R} \rho(x,T)\,\mathrm{d}x + \rho_R(M - TC_R). \tag{3.14}$$

Using equation (3.14) to further simplify equation (3.12) yields

$$\int_{TC_L}^{TC_R} \rho(x,T)\ \mathrm{d}x = T[f(\rho_L) - f(\rho_R) + \rho_R C_R - \rho_L C_L]. \tag{3.15}$$

Thus the integral of the exact solution to the Riemann problem between the slowest and fastest wave speeds is a constant given by the right-hand side of equation (3.15). Now we can use equation (3.15) to find the flux across a cell interface by splitting it into two integrals. The first integral is over the left side of the control volume from $[0, TC_L]$ leading to

$$\int_{TC_L}^{0} \rho(x,T)\ \mathrm{d}x = T[f(\rho_L) - f(\rho(0,t)) - \rho_L C_L] \tag{3.16}$$

and the second from $[0, TC_R]$ producing,

$$\int_{0}^{TC_R} \rho(x,T)\ \mathrm{d}x = T[f(\rho(0,t)) - f(\rho_R) + \rho_R C_R]. \tag{3.17}$$

Finally, rearranging (3.16) to solve for the flux across $x = 0$ leads to

$$f(\rho(0,t)) = f(\rho_L) - C_L\rho_L - \frac{1}{T}\int_{TC_L}^{0} \rho(x,T)\ dx. \tag{3.18}$$

We can also write an equivalent statement by rearranging (3.17) leading to

$$f(\rho(0,t)) = f(\rho_R) - C_R\rho_R + \frac{1}{T}\int_{0}^{TC_R} \rho(x,T)\ dx. \tag{3.19}$$

Equations (3.18) and (3.19) define the flux across the cell interface for any conservation law, and so the numerical flux must be consistent with these equations. We will derive the numerical flux for Roe's method based on this property.

Since (3.18) and (3.19) holds for any flux function we can write this property in terms of the linear PDE given by equation (3.9), where $f(\rho) = A\tilde{\rho}$. This leads to the following two forms:

$$A\tilde{\rho}(0,t) = A\rho_L - C_L\rho_L - \frac{1}{T}\int_{TC_L}^{0} \tilde{\rho}(x,T)\ dx \tag{3.20}$$

$$A\tilde{\rho}(0,t) = A\rho_R - C_R\rho_R + \frac{1}{T}\int_{0}^{TC_R} \tilde{\rho}(x,T)\ dx. \tag{3.21}$$

Rearranging to solve for the integrals in (3.20) and (3.21) yields

$$\frac{1}{T}\int_{TC_L}^{0} \rho(x,T)\ dx = A\rho_L - C_L\rho_L - A\tilde{\rho}(0,t) \tag{3.22}$$

$$\frac{1}{T}\int_{0}^{TC_R} \rho(x,T)\ dx = -A\rho_R + C_R\rho_R + A\tilde{\rho}(0,t). \tag{3.23}$$

At this point a subtle approximation is made. We define equations (3.18) and (3.19) to be the flux from the original nonlinear problem across a cell interface. Because (3.18) and (3.19) contain a potentially difficult integral to compute exactly, we will approximate these integrals with the integrals derived from the linear problem given by equations (3.22) and (3.23). This leads to the following,

$$f(\rho(0,t)) = f(\rho_L) + A[-\rho_L + \tilde{\rho}(0,T)] \tag{3.24}$$

and

$$f(\rho(0,t)) = f(\rho_R) - A[\rho_R - \tilde{\rho}(0,T)]. \tag{3.25}$$

Since the right-hand side is constant, the numerical flux (3.4) is easily derived from here. Notice we only need to provide the constant state along the cell interface $Q_{i-1/2}$ which in the scalar case is either Q_{i-1} or Q_i. Using equation (3.24), the numerical flux is then given by

$$F^n_{i-1/2} = f(Q_L) + A(-Q_L + Q_{i-1/2}), \tag{3.26}$$

which is equivalent to using (3.25) leading to

$$F^n_{i-1/2} = f(Q_R) - A(Q_R - Q_{i-1/2}). \tag{3.27}$$

We have shown how do derive a Roe linearization for a scalar conservation law and determined the numerical flux given that all shock or rarefaction waves are either fully right-going or fully left-going. We will now describe the fix that is needed in the case of a transonic rarefaction.

3.3.1 Entropy Fix

Figure 3.5 (a) shows the results from applying Roe's method without an entropy fix being applied in the transonic rarefaction case. The solution produced is a non-physical, entropy violating solution sometimes called an expansion-shock. For this reason an entropy fix is required. There are many types of entropy fixes and in this section we will focus on the Harten-Hyman entropy fix [24]. We will use the notation Q_L to denote the density to the left of the trailing rarefaction wave and Q_R to denote the density to the right of the leading rarefaction wave.

The idea behind this fix is to split the single jump propagating at speed A into two smaller jumps propagating at speeds $f'(Q_L)$ and $f'(Q_R)$ as shown in Figure 3.6. These

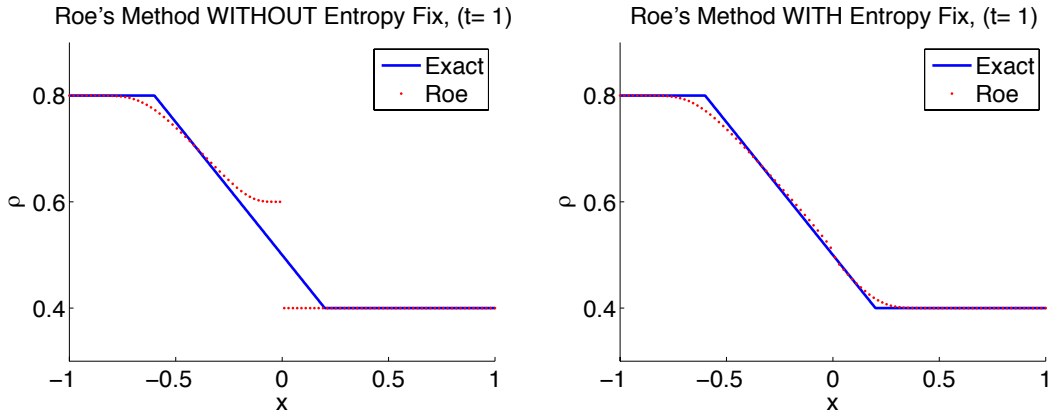

(a) (b)

Figure 3.5: The figures above show the computed solution to a Riemann problem using Roe's method with and without an entropy fix. It is clear that without an entropy fix non-physical solutions will be attained. It is interesting to note that a slight bump in (b) at $x = 0$ is sometimes referred to as the sonic glitch and it vanishes as $\Delta x \to 0$ [23].

two jumps are separated by a constant intermediate state Q_S. Using the integral form of the PDE we can show that Q_S should be chosen such that it produces the same change in density in the cell as the linearized problem. Figure 3.6 demonstrates that the addition of the areas contained in the blue rectangles, with the light blue area being negative, must equal the area contained by the red rectangle. This is written as,

$$f'(Q_L)(Q_L - Q_S) + f'(Q_R)(Q_S - Q_R) = A(Q_L - Q_R). \tag{3.28}$$

Equation (3.28) can then be rearranged to solve for Q_S:

$$Q_S = \frac{Q_L(A - f'(Q_L)) + Q_R(f'(Q_R) - A)}{f'(Q_R) - f'(Q_L)} \tag{3.29}$$

With this information, the numerical flux for the transonic case is calculated by substituting $Q_S = Q_{i-1/2}$ into either of equations (3.26) or (3.27). Care must be taken here though, since we replaced the single wave propagating at speed A with two waves propagating at speeds $f'(Q_L)$ and $f'(Q_R)$ the numerical flux must reflect the fact that the jumps $-Q_L + Q_S$ and $Q_R - Q_S$ are moving at these new speeds. Thus, in the transonic case

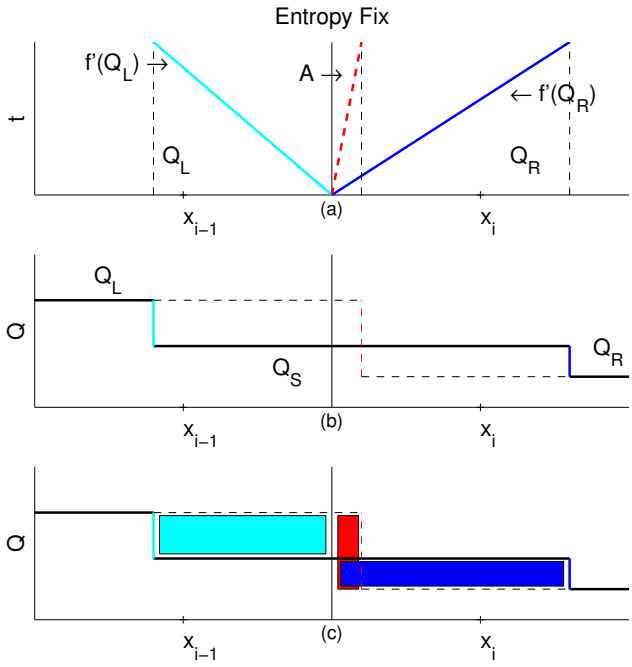

Figure 3.6: Given that the original problem has a transonic rarefaction, replace A (red line) with two waves traveling at the slowest and fastest speed in the rarefaction (blue lines). Then approximate the constant state along the cell interface by finding a Q_S such that the density is conserved between the linear problem using A and the problem using the rarefaction wave speeds $f'(Q_L)$ and $f'(Q_R)$. i.e. the sum of the areas in the blue boxes must equal the area in the red box.

$F^n_{i-1/2} \neq f(Q_L) + A(-Q_L + Q_S)$, but rather:

$$F^n_{i-1/2} = f(Q_L) + f'(Q_L)(-Q_L + Q_S) \tag{3.30}$$

$$= f(Q_R) - f'(Q_R)(Q_R - Q_S). \tag{3.31}$$

Now the implementation of Roe's method for scalar conservation laws can be summed up compactly as follows:

1. If A is transonic then $F^n_{i-1/2} = f(Q_L) + f'(Q_L)(-Q_L + Q_S)$.
2. If A is right-going then $F^n_{i-1/2} = f(Q_L)$.
3. And if A is left-going then $F^n_{i-1/2} = f(Q_R)$,

where A is given by equation (3.10). This concludes the formulation of Roe's method.

Chapter 4

Two-Class Traffic Flow

The goal of this section is to extend the LWR model to account for two classes of drivers so that the model includes a density evolution equation for each type. One can think of this as a scenario for a group of drivers who are late for work in the morning (fast drivers) sharing a road with a group of drivers who are simply out to enjoy the scenery (slow drivers). We will begin by introducing the governing equations for two-class flow.

4.1 Governing Equations

Let ρ_1 be the density of fast drivers seeking to move at a maximum speed α_1. Similarly, ρ_2 will be the density of slow drivers seeking to move at a maximum speed α_2. The densities will be represented in vector form as $\vec{q} = [\rho_1, \rho_2]^T$. It will also be useful to talk about the total density, as one's velocity should depend on the total density $\rho = \rho_1 + \rho_2$ in the vicinity and not just the density of one's own class [25, 30, 29] . The velocity function for the k^{th} class is then given by,

$$v_k(\vec{q}) = \alpha_k \left(1 - \frac{\rho}{\rho_m}\right). \tag{4.1}$$

And so, the full equations governing two-class flow with $f_k(\vec{q}) = v_k \rho_k$ are,

$$\partial_t \rho_1 + \partial_x \left[\alpha_1 \rho_1 \left(1 - \frac{\rho}{\rho_m}\right)\right] = 0, \tag{4.2}$$

$$\partial_t \rho_2 + \partial_x \left[\alpha_2 \rho_2 \left(1 - \frac{\rho}{\rho_m}\right)\right] = 0. \tag{4.3}$$

By non-dimensionalizing these equations the above system can be written in terms of only a single parameter. This will simplify the notation in our later discussion.

4.1.1 Non-Dimensionalization

Let $\tilde{\rho}_1 = \frac{\rho_1}{\rho_m}$, $\tilde{\rho}_2 = \frac{\rho_2}{\rho_m}$, $\tilde{t} = \frac{t}{T}$, $\tilde{x} = \frac{x}{L}$, then the partial derivatives become

$$\frac{\partial}{\partial t} = \frac{\partial \tilde{t}}{\partial t}\frac{\partial}{\partial \tilde{t}} = \frac{1}{T}\frac{\partial}{\partial \tilde{t}}$$
$$\frac{\partial}{\partial x} = \frac{\partial \tilde{x}}{\partial x}\frac{\partial}{\partial \tilde{t}} = \frac{1}{L}\frac{\partial}{\partial \tilde{x}}.$$

Dropping the tilde's and substituting into the original equations leads to

$$\partial_t \rho_1 + \alpha_1 \frac{T}{L}\partial_x[\rho_1(1-\rho)] = 0$$
$$\partial_t \rho_2 + \alpha_2 \frac{T}{L}\partial_x[\rho_2(1-\rho)] = 0.$$

Finally, we simplify the equations by choosing the time scale T so that $\frac{T\alpha_1}{L} = 1$ and then define $\frac{\alpha_2}{\alpha_1} = \bar{\alpha}$. The system in non-dimensionalized conservative form is given by,

$$\begin{aligned} \partial_t \rho_1 + \partial_x[\rho_1(1-\rho)] &= 0 \\ \partial_t \rho_2 + \partial_x[\bar{\alpha}\rho_2(1-\rho)] &= 0. \end{aligned} \tag{4.4}$$

The system can also be written in vector form as,

$$\partial_t \vec{q} + \partial_x \begin{bmatrix} \rho_1(1-\rho) \\ \bar{\alpha}\rho_2(1-\rho) \end{bmatrix} = 0, \tag{4.5}$$

and in nonconservative form as,

$$\partial_t \vec{q} + \begin{bmatrix} 1-2\rho_1-\rho_2 & -\rho_1 \\ -\bar{\alpha}\rho_2 & \bar{\alpha}(1-2\rho_2-\rho_1) \end{bmatrix} \partial_x \vec{q} = 0, \tag{4.6}$$

where the matrix is the Jacobian of the flux function, $\nabla \vec{f_{\vec{q}}}$ with eigenvalues

$$\lambda_{1,2} = \frac{1}{2}(\gamma_1 + \bar{\alpha}\gamma_2 \mp \sqrt{\eta}) \tag{4.7}$$

where,

$$\gamma_1 = 1-2\rho_1-\rho_2, \quad \gamma_2 = 1-2\rho_2-\rho_1 \quad \text{and} \quad \eta = (-\gamma_1 + \bar{\alpha}\gamma_2)^2 + 4\bar{\alpha}\rho_1\rho_2.$$

Clearly, both eigenvalues are real because $\eta > 0$ for all ρ_1, $\rho_2 > 0$ meaning our system is hyperbolic.

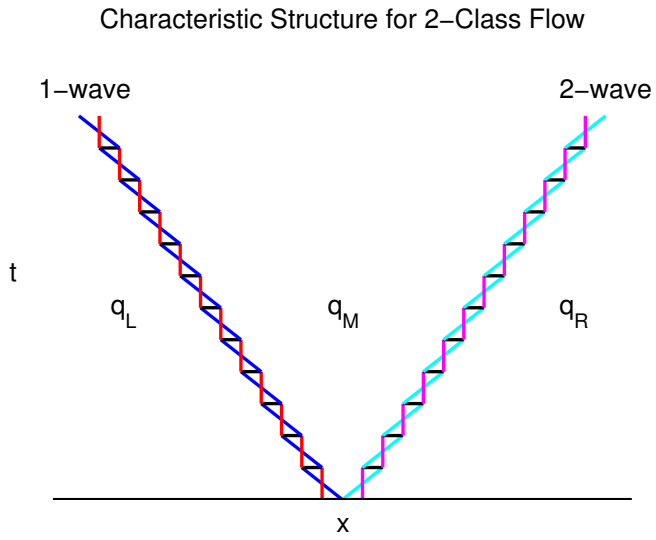

Figure 4.1: The wave structure for two-class flow includes two elementary waves, the 1-wave and the 2-wave, separated by a constant middle state $\vec{q}_M$.

4.2 The Riemann Problem for Two-Class Flow

For the remainder of this chapter the focus will be on finding the analytic solution to the Riemann problem for two-class flow. With this information we can confirm that the numerical results in Chapter 5 are correct, as well as gain a deeper understanding of Riemann solvers. The Riemann initial data for system (4.4) is given by,

$$\vec{q}(x,0) = \begin{cases} \vec{q}_L & \text{if } x \leq 0 \\ \vec{q}_R & \text{if } x > 0. \end{cases} \tag{4.8}$$

For a system of two hyperbolic conservation laws, the method of characteristics tells us that the solution to the Riemann problem will consist two elementary waves. These elementary waves will be some combination of shocks, rarefactions, or contacts (a degenerate wave). Our attention will focus on shocks and rarefactions since a contact is simply a degenerate shock. The important new idea for two-class flow is that between these two elementary waves a constant middle state $\vec{q}_M$ arises. We will define the elementary wave connecting the left state $\vec{q}_L$ to the middle state $\vec{q}_M$ as the 1-wave and the elementary wave connecting the middle state $\vec{q}_M$ to the right state $\vec{q}_R$ as the 2-wave. This characteristic

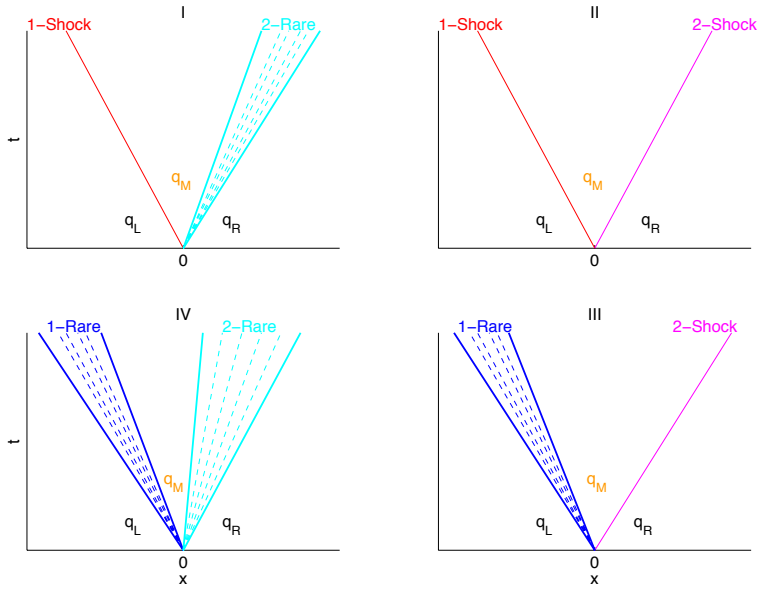

Figure 4.2: The four possible non-degenerate wave types are shown. (a) 1-shock, 2-rarefaction, (b) 1-shock, 2-shock, (c) 1-rarefaction, 2-rarefaction, and (d) 1-rarefaction, 2-shock. Notice that a constant middle state $\vec{q}_M$ separates the two waves in each case.

structure for two-class flow is shown in Figure 4.1 where the colored lines represent either of the two elementary waves types. Information about why systems take on this structure can be found in [16].

Figure 4.2 shows the four possible non-degenerate wave combinations for our problem. Given these four possibilities, two questions motivate the derivation of the exact solution. First, which one of the four wave types will occur given the left state $\vec{q}_L$ and the right state $\vec{q}_R$? And second, what is the value of the constant middle state $\vec{q}_M$ separating the two waves? Answering these questions will rely on an understanding of the Hugoniot locus for shocks and integral curves for rarefactions. This section will provide the analysis of the Hugoniot locus and integral curves for the 1-wave. In other words we will focus on finding all possible $\vec{q}_M$ that can connect to $\vec{q}_L$ by a 1-wave keeping in mind that the same procedure can be applied for the 2-wave.

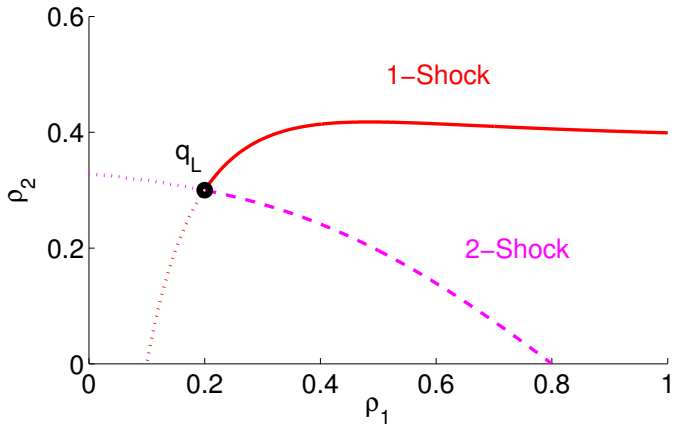

Figure 4.3: The red and magenta curves represent $\vec{q}_M$ satisfying the Rankine Hugoniot condition. The solid red curve shows the entropy satisfying $\vec{q}_M$ for a 1-shock. The dashed magenta curve shows the entropy satisfying $\vec{q}_M$ for a 2-shock.

4.2.1 The Hugoniot Locus for Shock Waves

The Hugoniot Locus or HL is defined as curves in $\rho_1\rho_2$-space that represent all possible $\vec{q}_M$ that can connect to the left or right state by a shock. From our knowledge of scalar hyperbolic PDEs a shock must satisfy two conditions. First, the shock speed must satisfy the Rankine Hugoniot condition (RHC),

$$s_*(\vec{q}_* - \vec{q}_M) = \vec{f}(\vec{q}_*) - \vec{f}(\vec{q}_M), \tag{4.9}$$

or in component form as,

$$\begin{aligned} s_*(\rho_{1*} - \rho_{1M}) &= \rho_{1*}(1 - \rho_*) - \rho_{1M}(1 - \rho_M), \\ s_*(\rho_{2*} - \rho_{2M}) &= \rho_{2*}\bar{\alpha}(1 - \rho_*) - \rho_{2M}\bar{\alpha}(1 - \rho_M). \end{aligned} \tag{4.10}$$

The * represents either the left or the right state (L or R), where s_L and s_R correspond to the speed of the 1-shock and the 2-shock respectively. Since we are focusing on the 1-wave the $*$ represents L. System (4.10) can be solved for ρ_{2M} in terms of ρ_{1M} to produce curves of $\vec{q}_M$ through $\vec{q}_L$ satisfying the RHC. These curves are shown in Figure 4.3 in red and magenta.

The second condition that a shock must satisfy is the entropy condition that was discussed in Chapter 2. The entropy condition for the 1-wave is such that the λ_1 characteristics collide to form a shock i.e. $\lambda_1(\vec{q}_L) > s_L > \lambda_1(\vec{q}_M)$ as in Figure 2.2. The fact that the 1-shock is only dependent on λ_1 follows from ordering of the eigenvalues. Further explanation of why this holds is given in the appendix.

The solid red line in Figure 4.3 represents all possible values of $\vec{q}_M$ that will connect to $\vec{q}_L$ by an entropy satisfying 1-shock. Along this curve the RHC and entropy condition are satisfied. The dashed magenta curve will play a clear role in section 4.2.3. It turns out to be the special curve in which $\vec{q}_M = \vec{q}_L$ and is therefore a curve of all possible $\vec{q}_R$ that will connect to $\vec{q}_M = \vec{q}_L$ through a 2-shock. From this definition this curve satisfies the entropy condition for a 2-shock i.e. $\lambda_2(\vec{q}_L) > s_R > \lambda_2(\vec{q}_M)$. Now that the possible middle states are known that will produce a 1-shock, we conduct a similar analysis for a 1-rarefaction.

4.2.2 Integral Curves for Rarefaction Waves

Just as the Hugoniot locus helps us determine the middle state when a shock is involved, integral curves help determine the middle state when a rarefaction is involved. From our knowledge of scalar hyperbolic PDEs a rarefaction must satisfy two conditions. The first condition is that the solution along a rarefaction must be the similarity solution. Making the change of variable $\vec{q}(x,t) = \vec{w}(x/t) = \vec{w}(\xi)$ leads to our system of conservation laws in the following form:

$$\nabla \vec{f}(\vec{w})\vec{w}' = \xi \vec{w}'. \tag{4.11}$$

For $\vec{w}' > 0$, equation (4.11) states that $\vec{w}'$ must be proportional to an eigenvector of $\nabla \vec{f}(\vec{w})$ and ξ must be the corresponding eigenvalue, i.e $\xi = \lambda_k(\vec{w}(\xi))$. Then

$$\vec{w}_k'(\xi) = a(\xi)\vec{m}_k(\vec{w}(\xi)), \tag{4.12}$$

where $a(\xi)$ depends on the parameterization of the integral curve, k represents the k^{th} wave and the eigenvectors $\vec{m}_1$ and $\vec{m}_2$ are given by,

$$\vec{m}_1 = \begin{bmatrix} \frac{1}{2\bar{\alpha}\rho_2}(\bar{\alpha}\gamma_2 - \gamma_1 + \sqrt{\eta}) \\ 1 \end{bmatrix} \text{ and } \vec{m}_2 = \begin{bmatrix} \frac{1}{2\bar{\alpha}\rho_2}(\bar{\alpha}\gamma_2 - \gamma_1 - \sqrt{\eta}) \\ 1 \end{bmatrix}. \tag{4.13}$$

Equation (4.12) states that eigenvectors are tangent to integral curves.

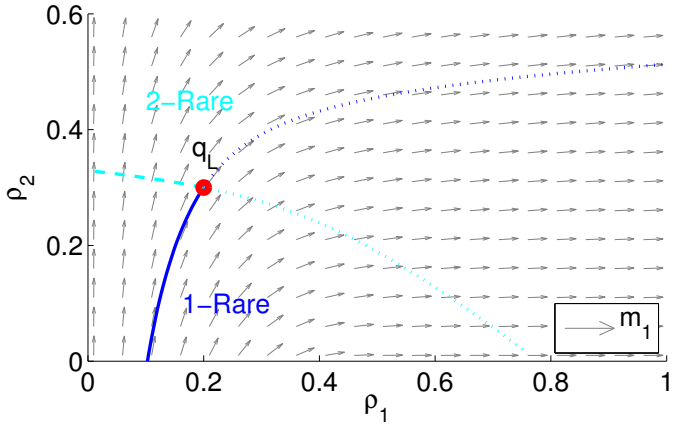

Figure 4.4: The blue and cyan curves represent $\vec{q}_M$ satisfying the similarity solution. The solid blue curve represents $\vec{q}_M$ such that λ_1 increases from the left to the middle state. And the dashed cyan curve represents $\vec{q}_M$ such that λ_2 increases from the left to the middle state. The gray arrows show how $\vec{m}_1$ eigenvectors are tangent to the blue integral curve.

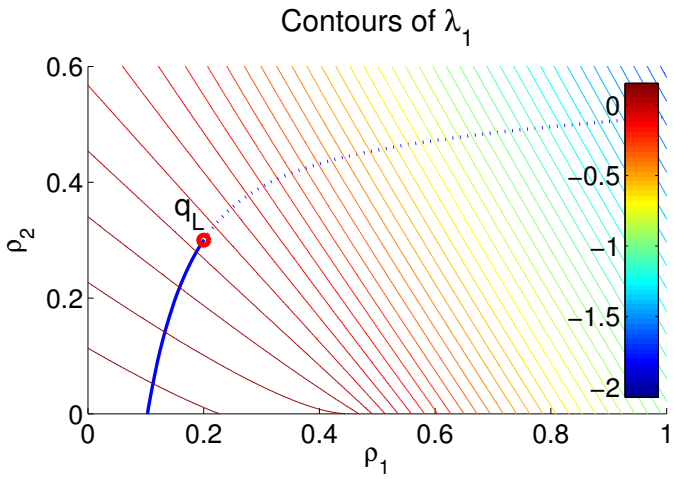

Figure 4.5: The contours of λ_1 and λ_2 are given for $\bar{\alpha} = 0.2$. The integral curves through $\vec{q}_*$ are plotted in black over the λ_1 and λ_2 contours. This figure demonstrates where both curves satisfy the conditions for a rarefaction i.e. $\lambda_1(\vec{q}_L) < \lambda_1(\vec{q}_M)$ and $\lambda_2(\vec{q}_L) < \lambda_2(\vec{q}_R)$ respectively.

To simplify system (4.12) we take the second equation in the system divided by the first producing a single ODE for ρ_2 as a function of ρ_1 yielding,

$$\frac{d\rho_2(\xi)}{d\rho_1(\xi)} = \frac{m_{2k}(\vec{w}(\xi))}{m_{1k}(\vec{w}(\xi))} \quad \text{and} \quad \rho_2(\rho_{1*}) = \rho_{2*}. \tag{4.14}$$

The solution to this ODE gives a curve in state space defining the k^{th} rarefaction solution $\vec{w}(\xi)$ between $\vec{q}_*$ and $\vec{q}_M$. Figure 4.4 shows the curves of $\vec{q}_M$ in blue and cyan that satisfy ODE (4.14). These curves are shown in blue and cyan. This figure also demonstrates how the eigenvector $\vec{m}_1$, shown in gray, runs tangent to the 1-rarefaction curve, shown in blue, as expected.

The second condition that a rarefaction must satisfy is the idea that characteristics diverge i.e. $\lambda_1(\vec{q}_L) < \lambda_1(\vec{q}_M)$ as discussed in Chapter 2. Figure 4.5 shows the contours of λ_1 demonstrating that the 1-rarefaction is chosen so that λ_1 is increasing from $\vec{q}_L$ to $\vec{q}_M$. The solid blue curve represents the $\vec{q}_M$ satisfying both the similarity solution and the entropy condition for a 1-rarefaction. The dashed cyan curve will play a clear role in section 4.2.3. It again turns out to be the special curve in which $\vec{q}_M = \vec{q}_L$ and is therefore a curve of all possible $\vec{q}_R$ that will connect to $\vec{q}_M = \vec{q}_L$ through a 2-rarefaction. From this definition this curve satisfies the second condition for a 2-rarefaction i.e. $\lambda_2(\vec{q}_L) < \lambda_2(\vec{q}_M)$. Now that the possible middle states are known that will produce a 1-rarefaction and a 1-shock we can put these ideas together to determine the wave combination and the middle state.

4.2.3 Putting it all together

We now refer to our original two questions: how to determine the wave combination and how to find the value of $\vec{q}_M$. Question 1 is answered by Figure 4.6 (a) which is simply Figures 4.3 and 4.4 combined. The solid curves represent all possible $\vec{q}_M$ and the dashed curves give the boundary for which $\vec{q}_M = \vec{q}_L$. These curves define four regions in state space corresponding to the four possible non-degenerate wave combinations. The location of $\vec{q}_R$ will determine how $\vec{q}_L$ connects to $\vec{q}_R$. For example, if $\vec{q}_R$ lives in region (III) then $\vec{q}_L$ will connect to $\vec{q}_M$ by a 1-rarefaction and $\vec{q}_M$ will connect to $\vec{q}_R$ by a 2-shock. Figure 4.6 (b) shows the integral and loci curves through $\vec{q}_L$ when $\vec{q}_L$ is in region 3. Question 2 is answered by Figure 4.7 (a) in which the two figures from 4.6 are overlaid. The middle state is then uniquely determined by the intersection of the 1-curve through $\vec{q}_L$ and the 2-curve through $\vec{q}_R$.

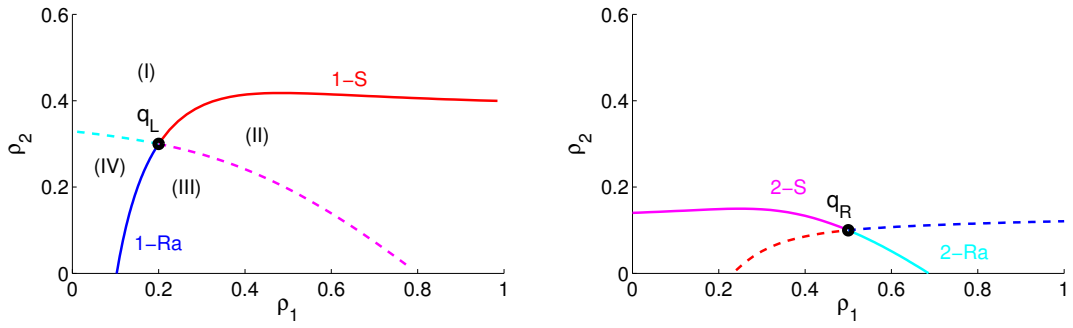

(a) (b)

Figure 4.6: (a) The four integral and loci curves split solution space into four regions where each region represents one of the four possible wave combinations. (b) The integral and loci curves are given for $\vec{q}_R$ where the solid curves represent the 2-wave and the dashed curves represent the 1-wave.

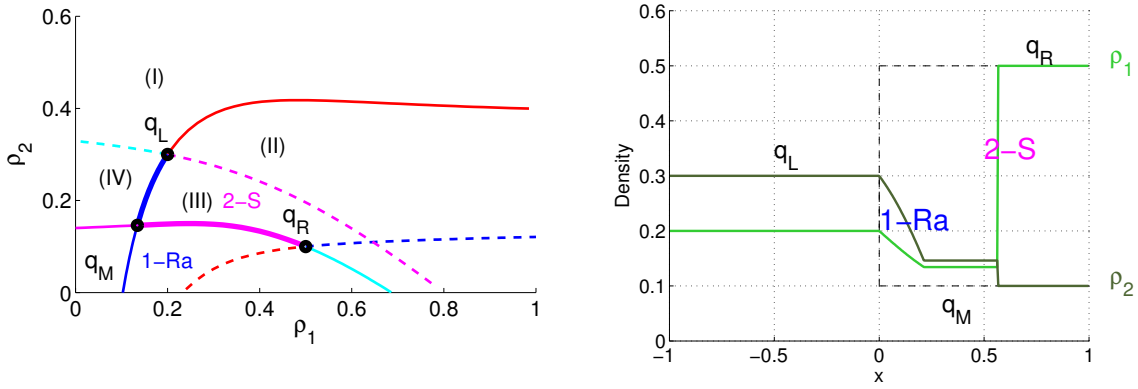

Figure 4.7: (a) Combining the figures from Figure 4.6 leads to the full solution to the Riemann problem in state space. The intersection of the 1-curve through $\vec{q}_L$ and the 2-curve through $\vec{q}_R$ gives $\vec{q}_M$. (b) The corresponding solution profile showing $\vec{q}_M$ and the two waves, 1-rarefaction and 2-shock.

Finally, Figure 4.6 (b) shows how the waves and middle state are translated from the ρ_1 vs. ρ_2 diagram to the density vs. space diagram. The wave speeds are either given by the characteristic speed for rarefactions, or by the RHC for shocks. And the solution along the rarefaction is given by the solution along the integral curve. This concludes the analysis for the full solution to the Riemann problem for two-class traffic flow. The next section will look at a special case where $\bar{\alpha} = 1$, providing additional insight to the analytical solution.

4.3 Riemann Problem for $\bar{\alpha} = 1$

In the case where $\bar{\alpha} = 1$ our problem is greatly simplified and so it is possible to demonstrate all the ideas above explicitly. We discuss this case because it summarizes the ideas of the Hugoniot locus and integral curves as well as highlights the third type of elementary wave, the degenerate contact wave keeping in mind that a contact is also possible in the general case. The eigenvalues and eigenvectors of this special system are the following:

$$\lambda_1 = 1 - 2\rho, \quad \vec{m}_1 = \begin{bmatrix} \rho_1 \\ \rho_2 \end{bmatrix}, \quad \lambda_2 = 1 - \rho, \quad \vec{m}_2 = \begin{bmatrix} 1 \\ -1 \end{bmatrix}. \tag{4.15}$$

Again we will focus on how the left state connects to the middle state through the 1-wave acknowledging that the same process can be applied for the 2-wave.

4.3.1 Hugoniot Locus for $\bar{\alpha} = 1$

We begin with the Hugoniot loci, curves of $\vec{q}_M$ satisfying the Rankine Hugoniot condition and entropy condition. With $\bar{\alpha} = 1$, we can derive the equations for the loci from system (4.10). Doing so leads to two straight lines given by

$$\rho_{2M} = \frac{\rho_{2L}}{\rho_{1L}} \rho_{1M} \tag{4.16}$$

and

$$\rho_{2M} = -\rho_{1M} + \rho_L. \tag{4.17}$$

We now look for sections of these two curves that satisfy the entropy condition for shocks. A 1-shock through $\vec{q}_L$ will satisfy $\lambda_1(\vec{q}_L) > s > \lambda_1(\vec{q}_M)$ and a 2-shock through $\vec{q}_L$ will satisfy $\lambda_2(\vec{q}_L) > s > \lambda_2(\vec{q}_M)$. Letting (4.16) be curve (I) and (4.17) be curve (II) we can now solve for λ_1, λ_2 and s along curves (I) and (II). Along curve (I)

$$\lambda_1(\vec{q}_M) = 1 - 2\left(1 + \frac{\rho_{2L}}{\rho_{1L}}\right)\rho_{1M}, \tag{4.18}$$

$$\lambda_2(\vec{q}_M) = 1 - \left(1 + \frac{\rho_{2L}}{\rho_{1L}}\right)\rho_{1M} \tag{4.19}$$

and

$$s = -\rho_{1M}\left(1 + \frac{\rho_{2L}}{\rho_{1L}}\right) + (1 - \rho_L). \tag{4.20}$$

And along curve (II)

$$\lambda_1(\vec{q}_M) = 1 - 2\rho_R, \tag{4.21}$$

$$\lambda_2(\vec{q}_R) = 1 - \rho_R \tag{4.22}$$

and

$$s = 1 - \rho_L. \tag{4.23}$$

We then find that a 1-shock is satisfied along curve (I) for

$$0 < \rho_{1L} < \rho_{1M}.$$

Notice that the location of the 1-shock is similar to the location in the general problem. For the 2-shock we find that $\lambda_2(\vec{q}_L) = s = \lambda_2(\vec{q}_M)$ everywhere along curve (II). The fact that equation there is an equality brings us to the idea of a third type of elementary wave called a contact wave. A contact wave is a discontinuity that travels at the characteristic speed [16]. Physically this means that the individual densities may be different in different constant states, but the total density remains the same. This tells us that when $\bar{\alpha} = 1$ the 2-wave will always be a contact wave. Figure 4.8 shows the entropy satisfying 1-shock and 2-contact curves through $\vec{q}_L$ when $\bar{\alpha} = 1$.

4.3.2 Integrals Curves for $\bar{\alpha} = 1$

To find the integral curves we apply equation (4.14) first for $\vec{m}_1$ to determine all possible $\vec{q}_M$ that will connect to $\vec{q}_L$ by a 1-rarefaction and second for $\vec{m}_2$ to determine all possible 2-rarefactions.

First we solve the ODE for the 1-rarefaction:

$$\frac{d\rho_2}{d\rho_1} = \frac{\rho_2}{\rho_1}, \quad \text{where} \quad \rho_2(\rho_{1L}) = \rho_{2L}, \tag{4.24}$$

which yields the integral curve,

$$\rho_2 = \frac{\rho_{2L}}{\rho_{1L}}\rho_1. \tag{4.25}$$

Along this curve the condition $\lambda_1(\vec{q}_L) < \lambda_1(\vec{q}_M)$ is satisfied for $\rho_{1M} < \rho_{1L}$. Second we solve the ODE for the 2-rarefaction:

$$\frac{d\rho_2}{d\rho_1} = -1, \quad \text{where} \quad \rho_2(\rho_{1R}) = \rho_{2R}. \tag{4.26}$$

which produces,

$$\rho_2 = -\rho_1 + \rho_R. \tag{4.27}$$

Along this curve the condition $\lambda_2(\vec{q}_L) < \lambda_2(\vec{q}_R)$ is never true. In fact, just as in the shock case, $\lambda_2(\vec{q}_L) = \lambda_2(\vec{q}_R)$. This means that the characteristics $\lambda_2(\vec{q}_L)$ and $\lambda_2(\vec{q}_R)$ are parallel just as in a linear problem. For this reason, we call the 2-wave a linearly degenerate contact. The entropy satisfying integral curves are shown in Figure 4.8.

In general, we can determine if a wave is linearly degenerate by showing that the change in λ_k along an integral curve is identically zero. If an integral curve is parameterized by $\vec{w}(\xi)$ then,

$$\frac{d}{d\xi}\lambda_k(\vec{w}(\xi)) = \nabla\lambda_k(\vec{w}) \cdot \vec{w}'(\xi) = 0.$$

Since an integral curve is always in the direction of the k^{th} eigenvector then,

$$\nabla\lambda_k(\vec{w}) \cdot \vec{w}'(\xi) = \nabla\lambda_k \cdot \vec{m}_k = 0. \tag{4.28}$$

If equation (4.28) does not equal zero, then we say that the k^{th} wave is genuinely nonlinear [16]. Computing equation (4.28) for the special case $\bar{\alpha} = 1$ for the 1-wave we find

$$\nabla\lambda_1 \cdot \vec{m}_1 = \begin{bmatrix} -2 \\ -2 \end{bmatrix} \cdot \begin{bmatrix} \rho_1 \\ \rho_2 \end{bmatrix} \neq 0.$$

And computing equation (4.28) for the 2-wave we find

$$\nabla\lambda_2 \cdot \vec{m}_2 = \begin{bmatrix} -1 \\ -1 \end{bmatrix} \cdot \begin{bmatrix} 1 \\ -1 \end{bmatrix} = 0.$$

Therefore the 2-wave is always a contact.

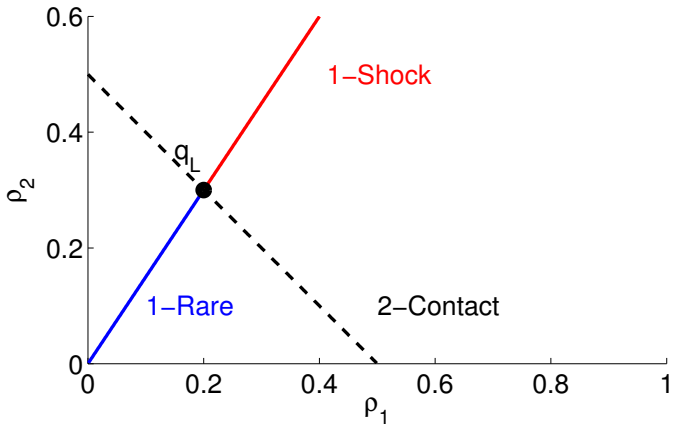

Figure 4.8: Hugoniot locus and integral curves though $\vec{q}_L$ for $\bar{\alpha} = 1$

Chapter 5

Numerics of Multi-Class Traffic Flow

Chapter 4 determined the exact solution to the Riemann problem for two classes of drivers. This information can be incorporated into a numerical scheme such as Godunov's method described in chapter 3, where the value in each cell is updated by finding the exact flux along the cell interface $x_{i-1/2}$. However, computing the exact solution at each cell interface can be computationally expensive, especially if the goal is to move toward more classes. Roe's method gives an alternative to finding the exact solution of a nonlinear PDE and instead finds the solution to a related but approximate linear problem. This section will first describe the Riemann problem for linear systems, then explain a way to approximate the nonlinear problem with a linear one. The Roe solver will be described for systems and specifically derived for multi-class traffic flow.

5.1 Riemann Problem for Linear Systems

The Riemann problem for a linear system is written as

$$\vec{q}_t + A\vec{q}_x = 0$$

with initial data

$$\vec{q}(x,0) = \begin{cases} \vec{q}_L & \text{if } x \leq 0, \\ \vec{q}_R & \text{if } x > 0, \end{cases}$$

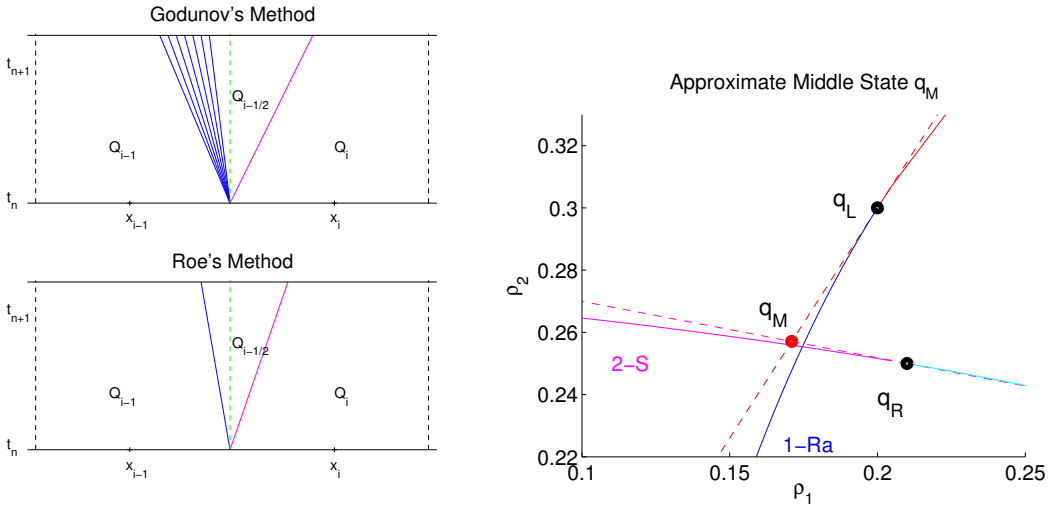

(a) (b)

Figure 5.1: These two plots demonstrates how the characteristics of the exact problem change when the problem is linearized. The left-going rarefaction in (a) reduces to a single discontinuity that is also left-going. While the right-going shock, shown in magenta, remains a right-going shock, usually with a different speed. The black dashed lines show the cell interfaces. In this case the constant solution along the vertical cell interface is the middle state $\vec{q}_M$. The corresponding plot in the $\rho_1\rho_2$-plane shows how to find q_M for both the exact and linear problem. $\vec{q}_M$ is the middle state corresponding to the approximate Riemann solution found by the intersection of the eigenvectors of A.

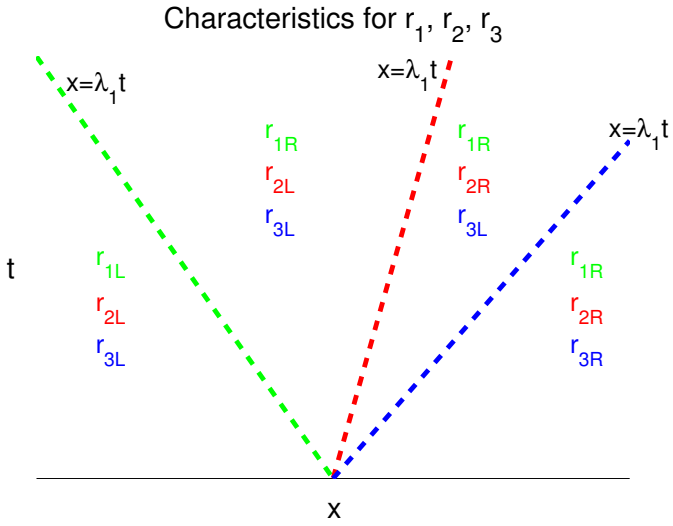

Figure 5.2: Characteristics are given for a system of 3 linear equations. Because the system is diagonalized the equations are decoupled and each component of $\vec{r}$ depends only on its corresponding characteristic. i.e. the solution for r_1 in the xt-plane is determined by the characteristic speed λ_1.

where A is an $n \times n$ matrix with constant entries. If A is diagonalizable, then it has an eigenvalue decomposition $A = PDP^{-1}$, where D is the diagonal matrix of eigenvalues $(\lambda_1 \leq ... \leq \lambda_n)$ and the columns of P are the corresponding eigenvectors $(\vec{m}_1, ..., \vec{m}_n)$. Making the change of variable $\vec{q} = P\vec{r}$, the PDE simplifies to a decoupled system of linear equations:

$$\vec{r}_t + D\vec{r}_x = 0$$

with initial data

$$\vec{r}(x,0) = \begin{cases} \vec{r}_L & \text{if } x \leq 0, \\ \vec{r}_R & \text{if } x > 0. \end{cases}$$

where $\vec{r}_L = P^{-1}q_L$ and $r_R = P^{-1}q_R$.

Figure 5.2 shows the characteristics and the solution in each region for a system of $n = 3$ linear PDEs. In each region, the solution $\vec{q}(x,t)$ can be found by the matrix-vector multiplication $\vec{q} = P\vec{r}$. Furthermore, $\vec{q}$ can be written as a linear combination of the n

eigenvectors $\vec{m}_k$, where $k = 1, ..., n$ as

$$\vec{q}(x,t) = P\vec{r}(x,t) = \sum_{k=1}^{n} r_k \vec{m}_k.$$

It will prove useful to express the total jump in $\vec{q}$ from the right to the left state, in terms of the jump across each of the k waves. Doing this yields

$$\begin{aligned}\vec{q}_R - \vec{q}_L &= P\vec{r}_R - P\vec{r}_L \\ &= \sum_{k=1}^{n} (r_{kR} - r_{kL})\vec{m}_k \\ &= \sum_{k=1}^{n} W_k\end{aligned}$$

where $W_k = (r_{kR} - r_{kL})\vec{m}_k$ is the jump in the solution $\vec{q}$ across the k^{th} wave. Any constant intermediate state can be found simply by adding the jump across successive waves to the left state, or alternately by subtracting successive jumps from the right state yielding

$$\vec{q}(x,t) = \vec{q}_L + \sum_{k:x \geq \lambda_k t} W_k \tag{5.1}$$

$$= \vec{q}_R - \sum_{k:x < \lambda_k t} W_k. \tag{5.2}$$

This idea of determining a constant middle state by adding jumps in the solution across successive waves will be used in our numerical method once we approximate the nonlinear traffic model with a linear system of equations. Next we will discuss how the Roe linearization is obtained.

5.2 Roe Linearization for Systems

Recall in chapter 3 that we derived A, an approximation to the characteristic speed $f'(\rho)$ for a scalar hyperbolic equation. For systems, this linearization is equivalent to finding an approximation to $\nabla \vec{f}(\vec{q})$, the Jacobian matrix. Roe determined that for the linear problem to be consistent with the nonlinear one, this approximate Jacobian matrix A must satisfy 3 conditions:

1. A is diagonalizable with real eigenvalues, that is, the linearized system remains hyperbolic.

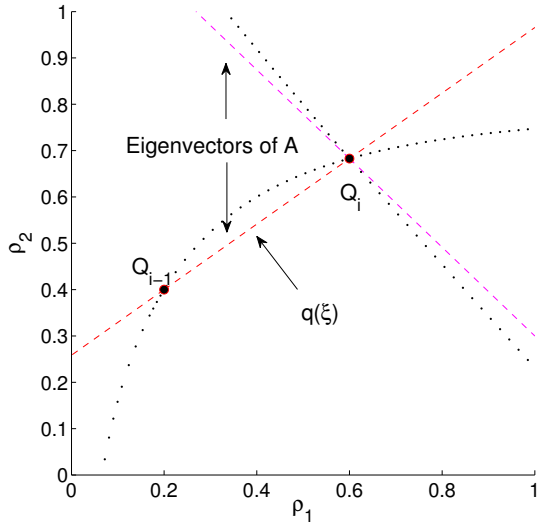

Figure 5.3: Case where a single shock wave connects state Q_{i-1} to Q_i in the original nonlinear problem, shown by the black curve. The red and magenta lines are the eigenvectors of A showing that the eigenvector also connects Q_{i-1} to Q_i by a single wave. $\vec{q}(\xi)$ is the parameterization of the straight line path along the eigenvector from Q_{i-1} to Q_i.

2. $A(Q_{i-1}, Q_i) \to \nabla \vec{f}(\vec{q})$ as Q_{i-1} and $Q_i \to \vec{q}$, which is a consistency condition for smooth flow.

3. $A(Q_{i-1} - Q_i) = \vec{f}(Q_{i-1}) - \vec{f}(Q_i)$, which enforces consistency for shocks.

To find a matrix A satisfying these three properties, Roe used the argument that "near a shock wave the Riemann problems arising at cell interfaces will typically have a large jump in at most one wave family" [16]. For this reason we require that when Q_{i-1} and Q_i are connected by a single shock wave in the original Riemann problem (i.e. there is no middle state), the approximate solution should also have a shock with the same speed. Thus, A should be constructed such that $Q_{i-1} - Q_i$ is an eigenvector and s, the exact shock speed, is the corresponding eigenvalue. This idea is illustrated in Figure 5.3 where the black curves represent the Hugoniot loci connecting the left state directly to the right state by a single shock. The red curve is an eigenvector of A and we require that it also connects Q_{i-1}

directly to Q_i. From this the following eigenvalue problem is obtained

$$A(Q_{i-1} - Q_i) = s(Q_{i-1} - Q_i). \tag{5.3}$$

Since s is the exact shock speed, s is given by the RHC as

$$s(Q_{i-1} - Q_i) = \vec{f}(Q_{i-1}) - \vec{f}(Q_i). \tag{5.4}$$

Equations (5.3) and (5.4) lead directly to condition 3:

$$A(Q_{i-1} - Q_i) = \vec{f}(Q_{i-1}) - \vec{f}(Q_i). \tag{5.5}$$

Another interpretation of equation (5.5) is that the jump in flux across the cell edge is equivalent for both the linear and nonlinear problem.

Now we would like a systematic way of deriving the matrix A from $\vec{f}$. One way is to integrate the Jacobian over a suitable path in state space between Q_{i-1} and Q_i. Let the parameterized curve $\vec{q}(\xi)$ be the path satisfying

$$\vec{q}(\xi) = (Q_{i-1} - Q_i)\xi + Q_i \quad \text{where} \quad 0 \leq \xi \leq 1. \tag{5.6}$$

Then, the right-hand side of equation (5.5) can be written as an integral along $\vec{q}(\xi)$

$$\begin{aligned} \vec{f}(Q_{i-1}) - \vec{f}(Q_i) &= \int_0^1 \frac{d\vec{f}(\vec{q}(\xi))}{d\xi}\, d\xi \\ &= \int_0^1 \frac{d\vec{f}(\vec{q})}{d\vec{q}} \vec{q}\,'(\xi)\, d\xi. \end{aligned}$$

Since $\vec{q}\,'(\xi) = (Q_{i-1} - Q_i)$ from equation (5.6) it follows that

$$\begin{aligned} \vec{f}(Q_{i-1}) - \vec{f}(Q_i) &= (Q_{i-1} - Q_i) \int_0^1 \frac{d\vec{f}(\vec{q})}{d\vec{q}}\, d\xi \\ &= (Q_{i-1} - Q_i) \int_0^1 J\, d\xi. \end{aligned}$$

Therefore, A is derived by finding the mean value of the Jacobian along the straight line connecting Q_{i-1} to Q_i.

This formulation of A guarantees that conditions 2 and 3 are satisfied, while condition 1 must be verified for the specific problem. For the multi-class traffic problem considered in this thesis, this method for finding A is very straightforward. However, in general, finding a suitable Roe linearization can be difficult, requiring a special change of variables that

has been obtained for only a few nonlinear systems (Euler equations and shallow water equations to name two). As a result, a number of alternatives to the Roe linearization have been proposed. For example, The Roe-Pike method eliminates the need to construct A and instead seeks to find averaged quantities of the primative variables ρ_i which are then used to evaluate the eigenvalues, eigenvectors and wave strengths directly [24].

5.3 Roe's Method

Recall that the general updating scheme for finite volume methods is given by

$$Q_i^{n+1} = Q_i^n + \frac{\Delta t}{\Delta x}(F_{i-1/2} - F_{i+1/2}) \tag{5.7}$$

where the numerical flux for systems is the same as described in chapter 3:

$$F_{i-1/2}^n = f(Q_L) + A(-Q_L + Q_{i-1/2}) \tag{5.8}$$

or equivalently,

$$F_{i-1/2}^n = f(Q_R) - A(Q_R - Q_{i-1/2}). \tag{5.9}$$

The ideas from section 5.1 can be applied to write the flux in another form. Since $-Q_L + Q_{i-1/2}$ is the the jump from the left state to the constant state along the cell interface, it can be written as

$$A(Q_{i-1/2} - Q_L) = \sum_{k:\lambda_k<0} AW_k \tag{5.10}$$

$$A(Q_R - Q_{i-1/2}) = \sum_{k:\lambda_k>0} AW_k. \tag{5.11}$$

where W_k is the jump across the k^{th} wave. Then, since $\vec{m}_k$ is an eigenvector of A, $A\vec{m}_k = \lambda_k\vec{m}_k$. The numerical flux for Roe's method for systems can then be written as

$$F_{i-1/2}^n = f(Q_L) + \sum_{k:\lambda_k<0} \lambda_k W_k \tag{5.12}$$

$$F_{i-1/2}^n = f(Q_R) - \sum_{k:\lambda_k>0} \lambda_k W_k. \tag{5.13}$$

As described in chapter 3, the approximate linear system will give non-physical solutions when a transonic rarefaction occurs. The next section will extend the entropy fix derived in chapter 3 for scalar problems to systems.

5.3.1 Entropy Fix

Remember that by linearizing the Jacobian matrix using Roe's method, we are essentially replacing all rarefaction waves with shocks. This is sufficient except if the k^{th} wave satisfies $\lambda_{kL} < 0 < \lambda_{kR}$, where λ_{kL} and λ_{kR} are the characteristic speeds to the left and right of the k^{th} wave, in which case the k^{th} wave is transonic. Suppose for example that the 1-wave is transonic. Then the wave speed to the left of the 1-wave is the simple case $\lambda_{1L} = \lambda_1(Q_L)$. To the right of the 1-wave $\lambda_{1R} = \lambda_1(Q_{1R}) = \lambda_1(Q_L + W_1)$, where Q_{1R} is found by adding the jump across the first wave W_k to the left state. Now the same logic can be used that was described in chapter 3. For this example, the consistency condition is written as

$$\lambda_{1L}(Q_L - Q_S) + \lambda_{1R}(Q_S - Q_{1R}) = \lambda_1(Q_L - Q_{1R}) \tag{5.14}$$

where λ_1 is the smallest eigenvalue of A. Equation (5.14) can be rearranged to solve for Q_S, the constant intermediate state between λ_{kL} and λ_{kR} given by

$$Q_S = \frac{Q_L(\lambda_1 - \lambda_{1L}) + Q_{1R}(\lambda_{1R} - \lambda_1)}{\lambda_{1R} - \lambda_{1L}}, \tag{5.15}$$

Thus, the numerical flux is written as

$$F^n_{i-1/2} = f(Q_L) + \lambda_{1L}(-Q_L + Q_S). \tag{5.16}$$

Rewriting (5.16) using the expression for Q_S yields

$$F^n_{i-1/2} = f(Q_L) + \lambda_{1L}\left(\frac{\lambda_{1R} - \lambda_1}{\lambda_{1R} - \lambda_{1L}}\right)(Q_{1R} - Q_L) \tag{5.17}$$

$$= f(Q_L) + \lambda_{1L}\left(\frac{\lambda_{1R} - \lambda_1}{\lambda_{1R} - \lambda_{1L}}\right)W_1. \tag{5.18}$$

5.4 Roe Solver for 2-Class Traffic Flow

We will now demonstrate Roe's method for our system of two equations. The first step is to find a Roe linearization of the Jacobian matrix

$$J = \begin{bmatrix} 1 - 2\rho_1 - \rho_2 & -\rho_1 \\ -\bar{\alpha}\rho_2 & \bar{\alpha}(1 - 2\rho_2 - \rho_1) \end{bmatrix}.$$

To do this we integrate each element of the matrix along the straight line connecting $\vec{q}_L$ to $\vec{q}_R$ parameterized by

$$\vec{q}(\xi) = (\vec{q}_R - \vec{q}_L)\xi + \vec{q}_L \quad \text{where} \quad 0 < \xi < 1 \tag{5.19}$$

leading to

$$A = \begin{bmatrix} \int_0^1 (1 - 2\rho_1(\xi) - \rho_2(\xi))d\xi & -\int_0^1 \rho_1(\xi)d\xi \\ -\int_0^1 \bar{\alpha}\rho_2(\xi)d\xi & \int_0^1 \bar{\alpha}(1 - 2\rho_2(\xi) - \rho_1(\xi))d\xi \end{bmatrix}.$$

As an example, we will provide the details for the integral of the first component.

$$\int_0^1 (1 - 2\rho_1(\xi) - \rho_2(\xi))d\xi = 1 - 2\left(\frac{1}{2}(\rho_{1L} + \rho_{1R})\right) - \frac{1}{2}(\rho_{2L} + \rho_{2R}).$$

Letting $\bar{\rho}_1 = \frac{1}{2}(\rho_{1L} + \rho_{1R})$ and $\bar{\rho}_2 = \frac{1}{2}(\rho_{2L} + \rho_{2R})$ and completing the other three integrals, the matrix A is given by

$$A = \begin{bmatrix} 1 - 2\bar{\rho}_1 - \bar{\rho}_2 & -\bar{\rho}_1 \\ -\bar{\alpha}\bar{\rho}_2 & \bar{\alpha}(1 - 2\bar{\rho}_2 - \bar{\rho}_1) \end{bmatrix}.$$

The eigenvalues and eigenvectors are

$$\lambda_{1,2} = \frac{1}{2}(\bar{\gamma}_1 + \bar{\alpha}\bar{\gamma}_2 \mp \sqrt{\bar{\eta}}) \tag{5.20}$$

and

$$\vec{m}_{1,2} = \begin{bmatrix} \frac{1}{2\bar{\alpha}\bar{\rho}_2}(\bar{\alpha}\bar{\gamma}_2 - \bar{\gamma}_1 \pm \sqrt{\bar{\eta}}) \\ 1 \end{bmatrix}$$

where

$$\bar{\gamma}_1 = 1 - 2\bar{\rho}_1 - \bar{\rho}_2, \quad \bar{\gamma}_2 = 1 - 2\bar{\rho}_2 - \bar{\rho}_1 \quad \text{and} \quad \bar{\eta} = (-\bar{\gamma}_1 + \bar{\alpha}\bar{\gamma}_2)^2 + 4\bar{\alpha}\bar{\rho}_1\bar{\rho}_2. \tag{5.21}$$

Note that A satisfies condition 1 since it has real eigenvalues.

Now that we have found a valid Roe linearization the next step is to determine the numerical flux which involves finding the jump W_k across the k^{th} wave. This calculation involves solving the linear system

$$\vec{q}_L - \vec{q}_R = P(\vec{r}_L - \vec{r}_R) \tag{5.22}$$

for $\vec{r}_L - \vec{r}_R$. Using this vector we can find W_k the jump across the k^{th} wave

$$W_k = (r_{kL} - r_{kR})\vec{m}_k. \tag{5.23}$$

As for the transonic case we only need to consider the 1-wave due to the fact that $\lambda_2 \geq 0$. Since $\lambda_2 = 0$ for $\bar{\rho} = \frac{1}{2}$ and $\bar{\rho} = 1$ and since $\lambda_2 > 0$ on $0 < \bar{\rho} < \frac{1}{2}$ and $\frac{1}{2} < \bar{\rho} < 1$ we claim that $\lambda_2 > 0$. This analysis shows that we only need an entropy fix for the 1-wave. Therefore,

for two-class flow there are only three cases for the approximate Riemann problem. In case 1, as shown in Figure 5.4 (a), all eigenvalues of A are right-going and so

$$F_{i-1/2} = f(Q_L). \tag{5.24}$$

In case 2, as shown in Figure 5.4 (b), λ_1 is left-going and λ_2 is right-going and so

$$F_{i-1/2} = f(Q_L) + \lambda_1(-Q_L + QM) = f(Q_L) + \lambda_1 W_1. \tag{5.25}$$

And in case 3, as shown in Figure 5.4 (c), λ_1 is transonic and so

$$F_{i-1/2} = f(Q_L) + \lambda_{1L}(-Q_L + QS) = f(Q_L) + \lambda_{1L}\left(\frac{\lambda_{1R} - \lambda_1}{\lambda_{1R} - \lambda_{1L}}\right) W_1. \tag{5.26}$$

5.5 CLAWPACK Simulations

All of the simulations that will be presented have been solved using the publicly available CLAWPACK package for solving hyperbolic PDEs using exact or approximate Riemann solvers. The user only needs to supply CLAWPACK with the eigenvalues and eigenvectors of the exact Jacobian, or Roe linearized matrix along with W_k and the entropy fix. Variable time stepping, boundary conditions and flux limiters are built in functions making this a relatively straightforward way of implementing a Roe solver. Details about this package can be found in [16].

5.5.1 Two-Class Simulations

In this section we will show the four solution profiles, one from each of the possible non-degenerate cases, discuss the convergence of our method and show that our results match a test case found in the literature. Figure 5.5 shows an example from each of the four possible non-degenerate cases produced from different Riemann initial data. The wave speeds produced by Roe's method match well with the exact solution. These simulations were all produced with $\bar{\alpha} = 0.5$, $T = 1$ and with $N = 300$ cells on the domain from $[-1, 1]$. Plot (c) in Figure 5.5 contains a transonic rarefaction in the 1-wave since the slowest wave in the rarefaction is moving to the left and the fastest wave in the rarefaction is moving to the right of the initial discontinuity. The sonic glitch is at $x = 0$ and will vanish as $dx \to 0$.

Now we will study the convergence of Roe's method. The convergence rate will be observed for a case with a discontinuous solution and another case with a smooth solution.

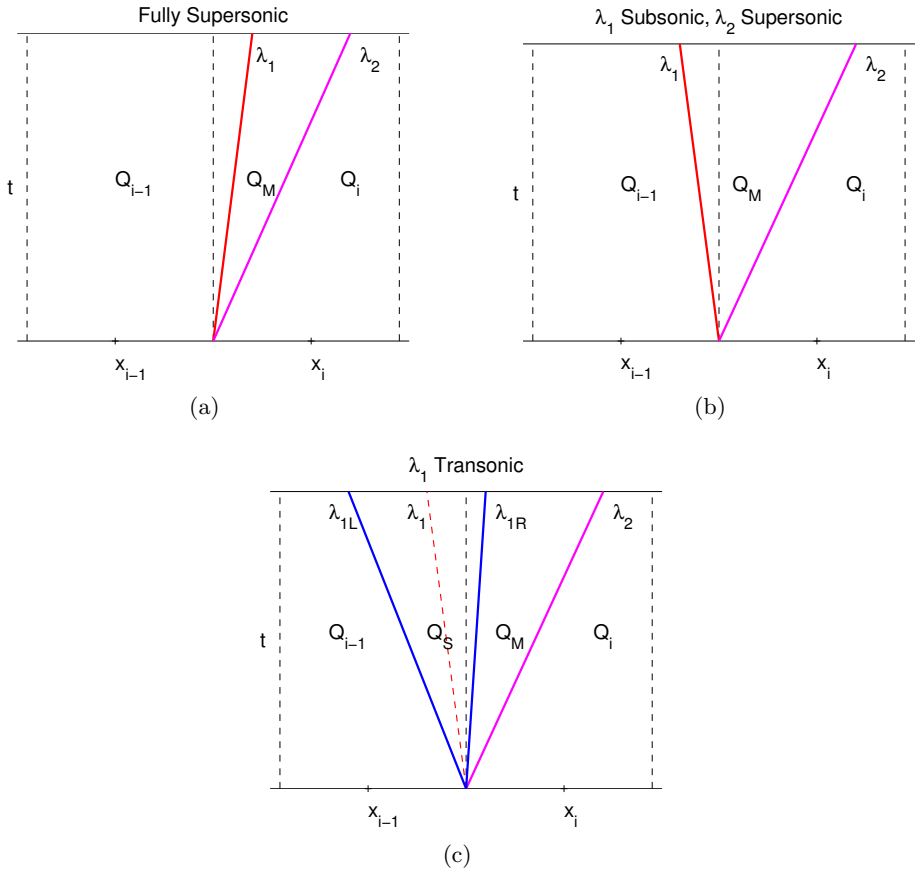

Figure 5.4: There are three scenarios that are possible for two-class traffic flow. In (a) the wave speeds are all right-going and thus $Q_{i-1/2} = Q_L$. (b) is the case where λ_1 is left-going and λ_2 is right-going leading to $Q_{i-1/2} = Q_M$. (c) shows that λ_1 is transonic which leads to $Q_{i-1/2} = Q_S$.

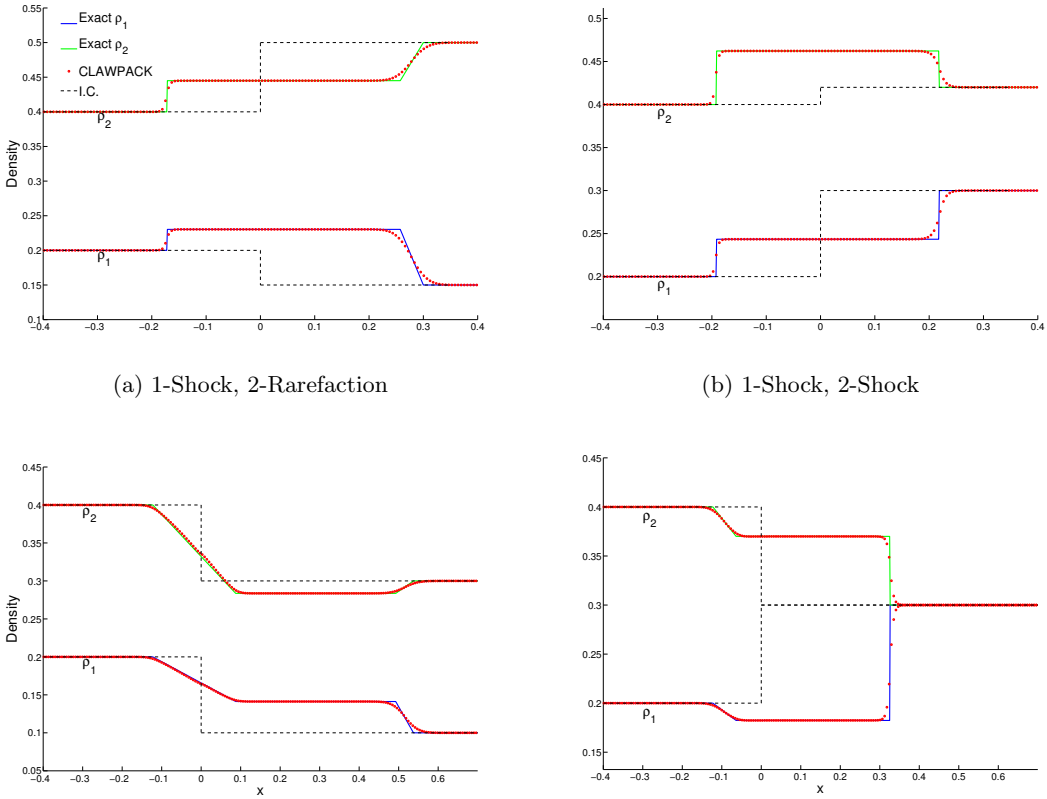

(a) 1-Shock, 2-Rarefaction

(b) 1-Shock, 2-Shock

(c) 1-Rarefaction, 2-Rarefaction

(d) 1-Transonic Rarefaction, 2-Shock

Figure 5.5: The solution profiles are shown for the four non-degenerate combinations of elementary waves discussed in chapter 4. The dashed black lines show the initial condition while the solid blue and green lines show the exact solution derived in section 4. The red dots represent the solution computed using a Roe method with second order corrections.

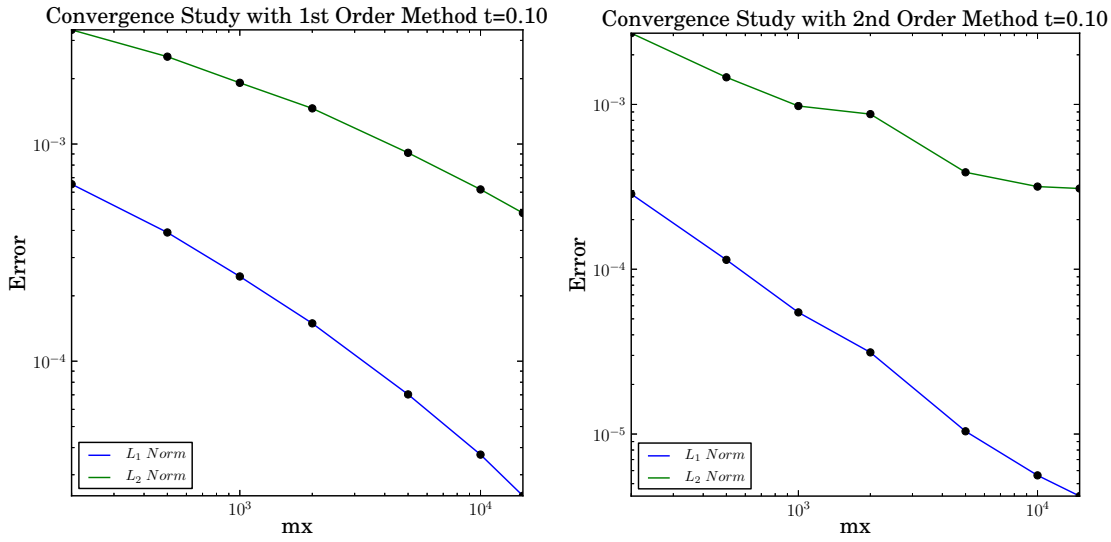

(a) $l_1 = 0.7$, $l_2 = 0.45$ (b) $l_1 = 0.99$, $l_2 = 0.52$

Figure 5.6: Convergence rates for discontinuous shock-rarefaction case. For (a) the first order method and (b) the second order method.

For each of these we will show how the convergence rates differ when CLAWPACK is run with and without higher order correction terms. One of CLAWPACKs built in functions is the ability for the user to choose the order of accuracy to be first or second. For all of the convergence plots we will use $N = [200, 500, 1000, 2000, 5000, 10000, 15000]$ and fixed time stepping with $dt = 0.0001$, the largest possible dt for the finest mesh.

To study the convergence of a nonlinear hyperbolic problem we will use the l_1 and l_2 norms so that the large errors that can occur near discontinuities are not being over emphasized as would be the case in the l_∞ norm. Figure 5.6 shows the convergence rates of the l_1 and l_2 norms found when applying both the first and second order methods in CLAWPACK. The initial condition is taken from Figure 5.5 plot (a) and is run to $T = 0.1$ on the domain from $[-0.5, 0.5]$. This shows that with the second order correction terms, our method is first order convergent in the l_1 norm for discontinuous solutions. When the second order corrections are not implemented, the convergence rate is considerably lower. Achieving the accuracy of the respective methods is only expected in regions of smooth flow and reductions of order are expected when discontinuities are present. However, the convergence rates here are still lower than expected and at this time we do not have an

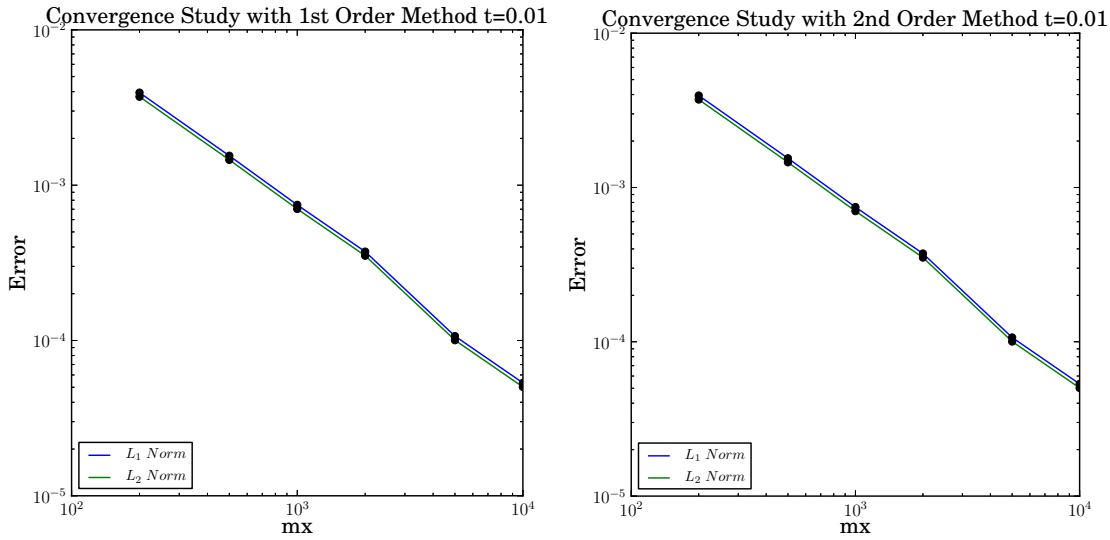

(a) $l_1 = 1.11$, $l_2 = 1.11$ (b) $l_1 = 1.11$, $l_2 = 1.11$

Figure 5.7: Convergence rates in the l_1 and l_2 norms for smooth flow.

explanation for this.

Now we examine the convergence of for a smooth solution with Gaussian initial data. The error will be found by comparing the numerical solution to one on grid with $N = 30000$. The results are shown in Figure 5.7 for the first and second order methods. The major difference in this study is that the l_2 rate is now the same as for the l_1 norm. The l_1 norm is slightly better although not as high as we would expect.

Our final simulation is one with initial data given in [28]. The initial condition is shown in blue in Figure 5.8 where the platoon on the left carries an even distribution of slow and fast drivers. In this scenario the fast drivers seek to drive at a maximum velocity that is twice that of the slow drivers, so that $\bar{\alpha} = 0.5$. We plot the solution after time $T = 1.2$ with $N = 800$ grid points on the domain from $[0, 2]$. Since the number of grid cells is not included in the paper, we cannot make any conclusions about the accuracy of one scheme relative to the other, however it is clear that we do reproduce the correct intermediate states and wave speeds.

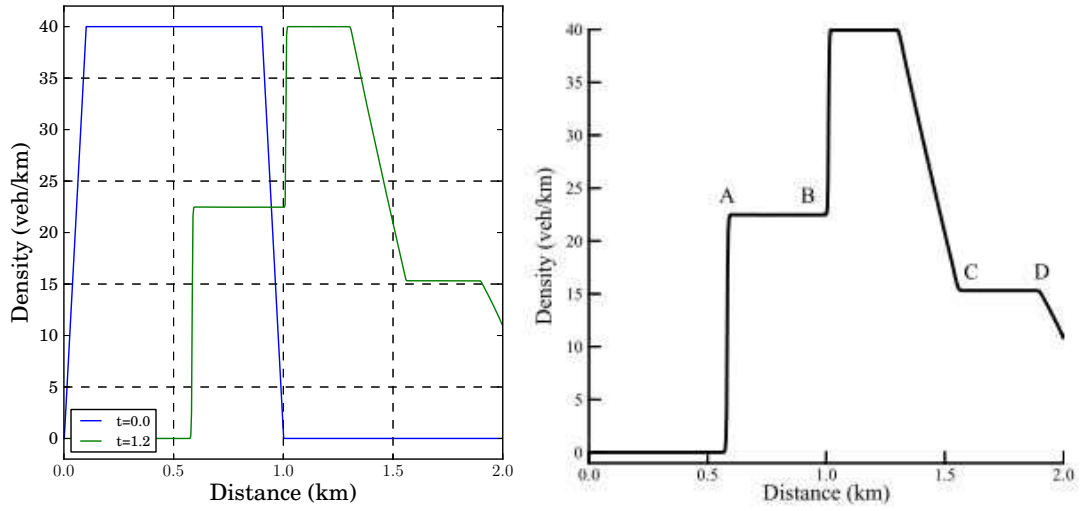

(a) Roe's Method (b) WENO Method

Figure 5.8: Comparison of Roe's method to a benchmark case that was computed using a 5^{th} order WENO scheme from [28].

5.5.2 Three-Class Simulations

For the system discussed in this thesis the Roe matrix can easily be generalized for any number of classes as:

$$A = \begin{bmatrix} \alpha_1(1-2\bar{\rho}-\bar{\rho}_1) & -\alpha_1\bar{\rho}_1 & \dots & -\alpha_1\bar{\rho}_1 \\ -\alpha_2\bar{\rho}_2 & \alpha_2(1-2\bar{\rho}-\bar{\rho}_2) & \dots & -\alpha_2\bar{\rho}_2 \\ \vdots & & \ddots & \vdots \\ -\alpha_{n-1}\bar{\rho}_{n-1} & \dots & \alpha_{n-1}(1-2\bar{\rho}-\bar{\rho}_{n-1}) & -\alpha_{n-1}\bar{\rho}_{n-1} \\ -\alpha_n\bar{\rho}_n & \dots & -\alpha_n\bar{\rho}_n & \alpha_n(1-2\bar{\rho}-\bar{\rho}_n) \end{bmatrix}$$

with $\bar{\rho}_i = 0.5(\rho_{iL} + \rho_{iR})$. Because of this structure the extension of our problem to more classes takes little extra work. The main difference from the two-class case is that the eigenvalues and eigenvectors can no longer be found explicitly and so we will have to implement an eigensolver into the code. This can be done through LAPACK. We will now focus on two examples studied by Zhang et. al [29] that solve the same multi-class traffic flow, but instead use a Lax-Freidrichs flux-splitting method with a 5th order WENO reconstruction and a 3rd order TVD Runge-Kutta time discretization.

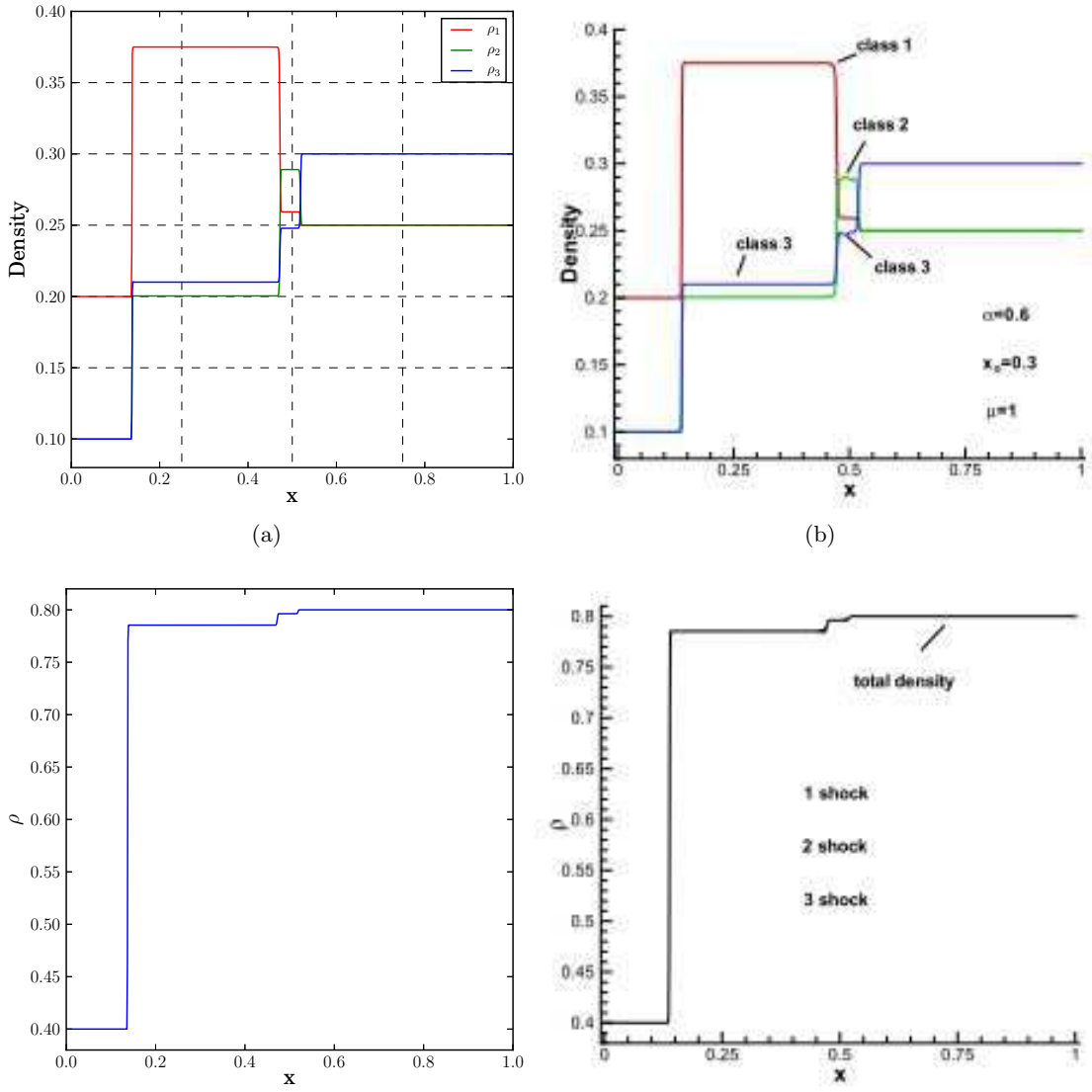

(a) (b)

(c) Roe's Method (d) FDM

Figure 5.9: Experiment 1: Comparison of our method to [29] for $\vec{q}_L = [0.2, 0.1, 0.1]$ and $\vec{q}_R = [0.25, 0.25, 0.3]$ with $N = 800$.

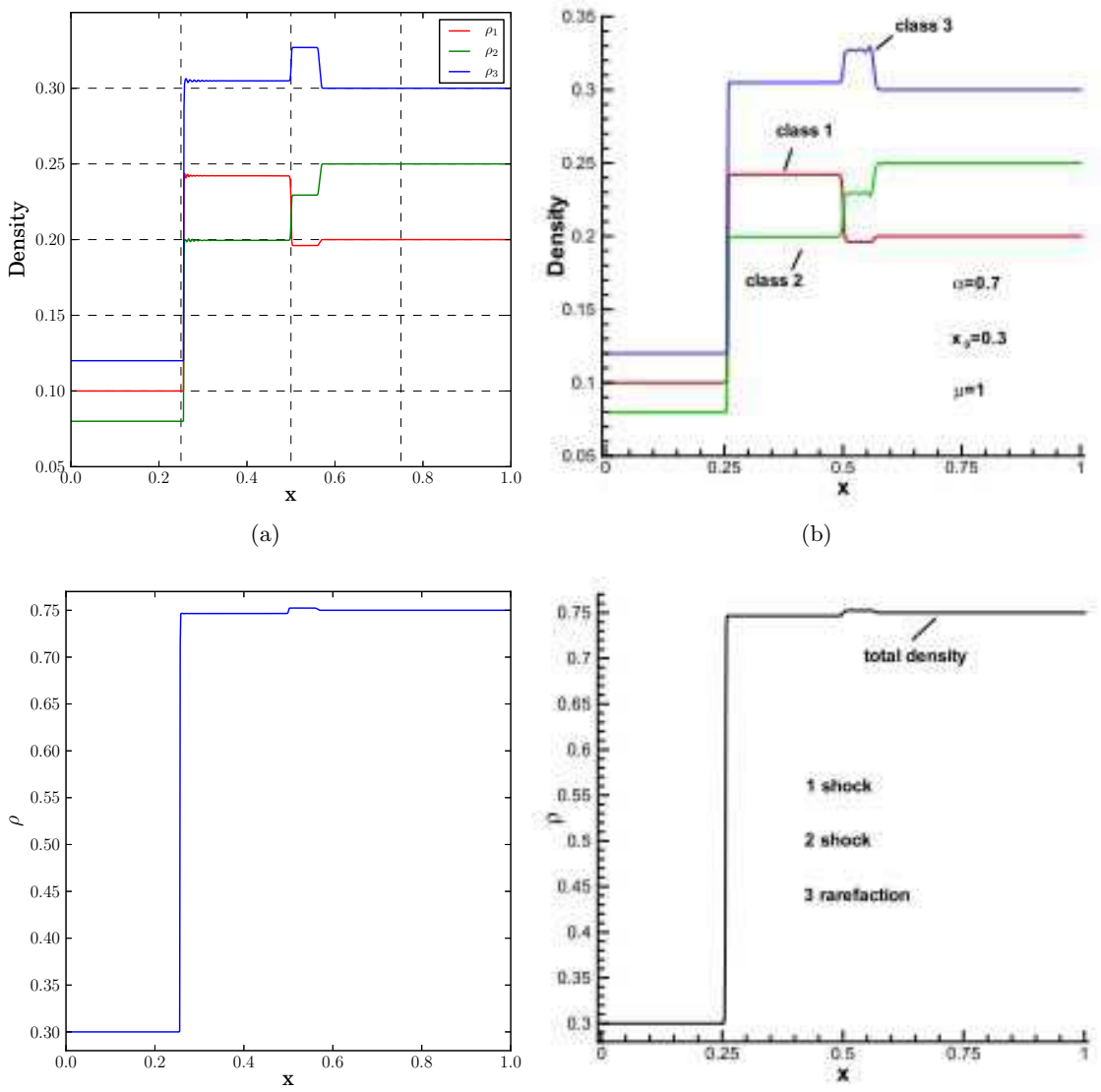

(a) (b)

(c) Roe's Method (d) FDM

Figure 5.10: Experiment 2: Comparison of our method to [29] for $\vec{q}_L = [0.1, 0.08, 0.12]$ and $\vec{q}_R = [0.2, 0.25, 0.3]$ with $N = 800$

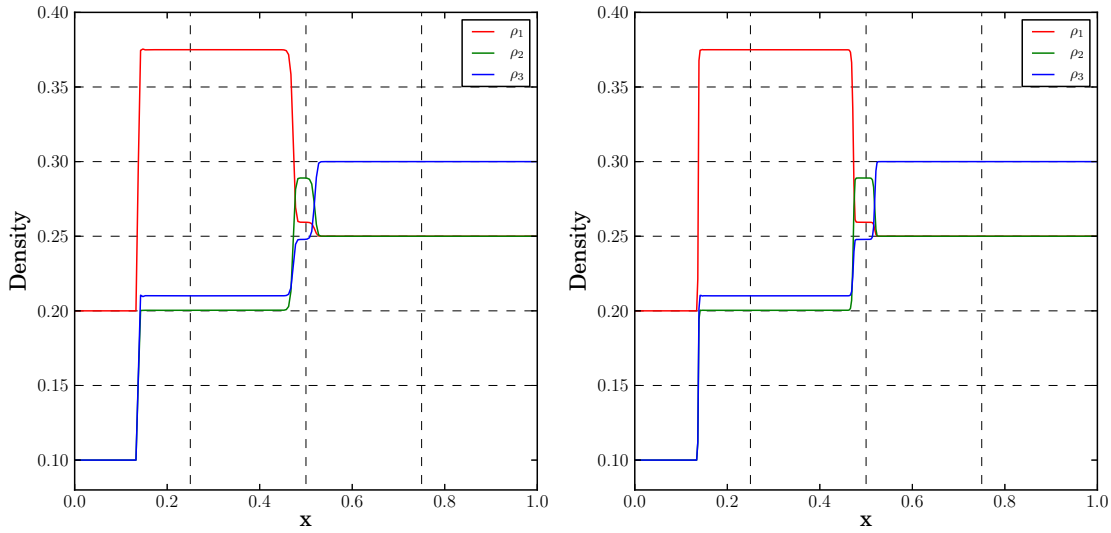

(a) $N = 200$ (b) $N = 400$

Figure 5.11: Results from experiment 1 with fewer grid cells.

For the following experiments the maximum velocities for each class are $\alpha_i = [0.6, 0.8, 1]$. The initial discontinuity of the Riemann problem is located at $x_0 = .3$ on the domain from $[0, 1]$ and the simulation is run with $T = 1.2$. The first experiment is an all shock scenario with $\vec{q}_L = [0.2, 0.1, 0.1]$ and $\vec{q}_R = [0.25, 0.25, 0.3]$. The second experiment is a 1-shock, 2-shock, 3-rarefaction scenario with $\vec{q}_L = [0.1, 0.08, 0.12]$, $\vec{q}_R = [0.2, 0.25, 0.3]$. Our code has been set to use variable time stepping and $N = 800$. Figures 5.9 and 5.10 show the individual densities and total density given by Roe's Method compared with [29] for the the two experiments. From observation Roe's method is outperforming Zhang et. al's. The middle states and shocks are better resolved by our method and in particular we see none of the oscillations seen in Zhang et. al.

Since we are seeing better results from our method, we would like to know for what grid size our results begin to look less resolved. Figure 5.11 shows the results for the same problem in Figure 5.9 with $N = 200$ and $N = 400$ grid cells. Figure 5.12 shows a zoomed in picture of a single class around the 2-shock and 3-shock with $N = [200, 400, 800, 1600]$. Clearly, the $N = 800$ solution has essentially converged.

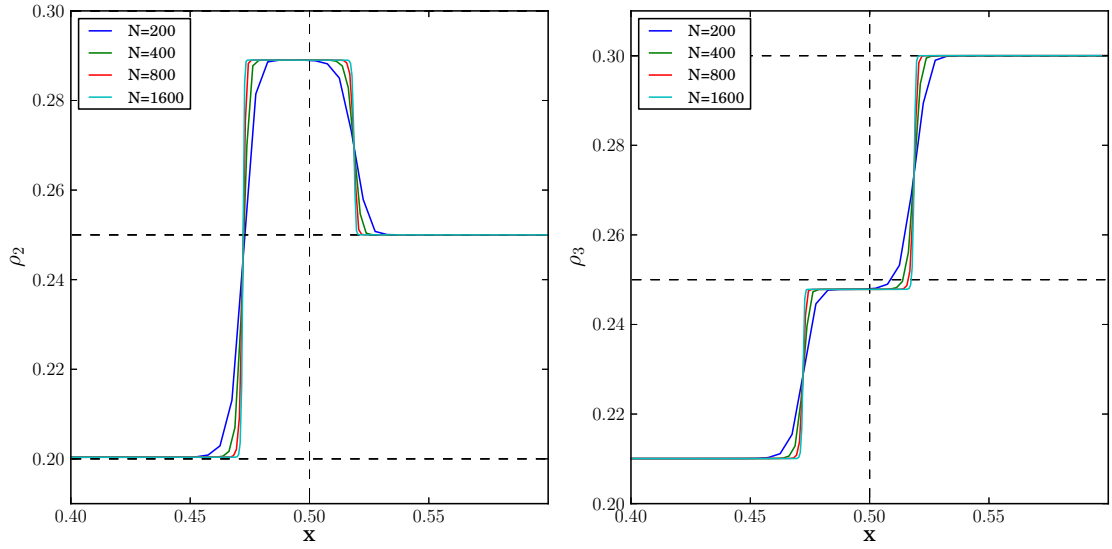

(a) ρ_2 (b) ρ_3

Figure 5.12: Zoomed in picture of the 2-shock and 3-shock from experiment 1. (a) and (b) show how ρ_2 and ρ_3 are resolved for grid sizes $N = [200, 400, 800, 1600]$.

5.5.3 Nine-Class Simulations

Finally, we wanted to test our scheme against the WENO scheme for a nine-class case. This is an interesting comparison because of the fact that this example was originally computed using the Lax-Friedrichs method in [25] which was so diffusive it smoothed out a staircase like behavior later illuminated by the WENO scheme in [28]. Note that this is a different WENO scheme than for the three-class comparison in the previous section.

Our nine-class experiment begins with an initial platoon shown in blue in Figure 5.8 where the initial total density is 40 and the maximum density is $\rho_m = 200$. In the platoon the individual classes have densities

$$\rho_i = [1.6, 3.2, 4.8, 6.4, 8, 6.4, 4.8, 3.2, 1.6]$$

and maximum velocities

$$\alpha_i = [60, 67.5, 75, 82.5, 90, 97.5, 105, 112.5, 120], \tag{5.27}$$

respectively. Our method is run with variable time stepping and $N = 1600$ on the domain from $[0, 2]$. Looking at the results in Figure 5.13 our method is capturing the middles states

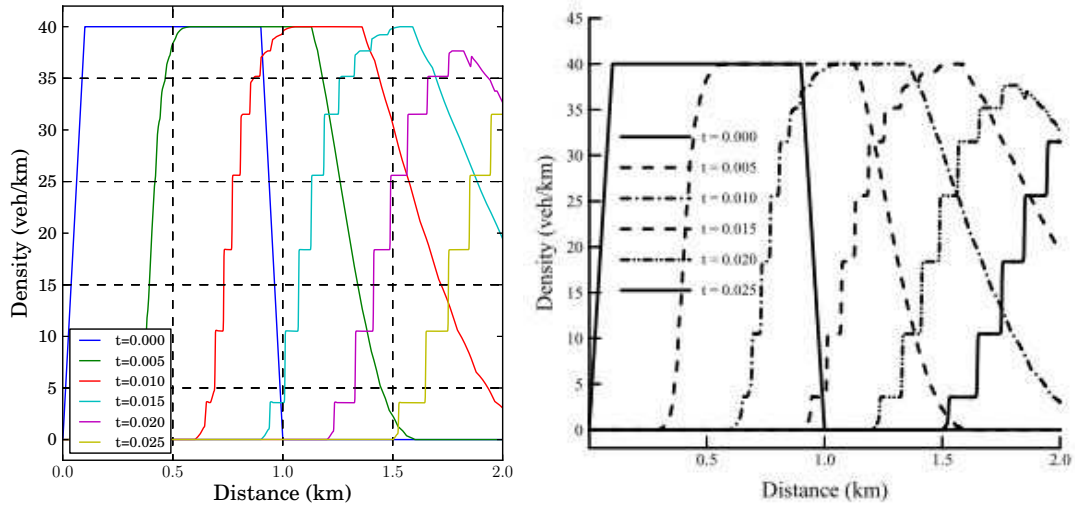

(a) Roe's Method (b) WENO Method

Figure 5.13: Comparison of Roe's method to a 5^{th} order WENO scheme at various times. The initial condition is given in blue.

and waves equally as well as the WENO scheme. We can zoom in on the peak of the solution profile at time $t = 0.02$ to determine how this region is resolved for different grid sizes. Figure 5.14 shows that our method will still capture this peak with $N = 400$ and $N = 800$ grid cells.

One final consideration is the transonic rarefaction case that was not considered by Zhang et. al. It is mentioned in [28] that the Godunov scheme is difficult, if not impossible, to compute when the eigenvalues change sign. For this reason we compute a case with a transonic rarefaction using Roe's method. The initial total density is 0.7 with the same class distribution as in the previous run. The max velocities are given by (5.27). In Figure 5.15 the sonic point at $x = 1$ is better resolved in the case with $N = 800$. These results are expected, however we remark that there is no analytical solution to compare to.

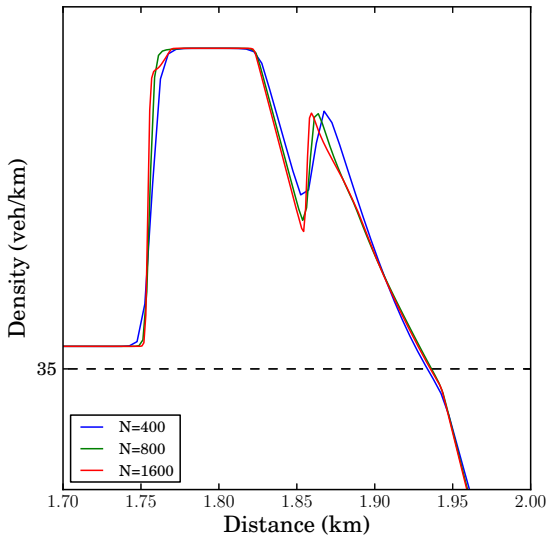

Figure 5.14: Zoomed in picture on the peak of the solution profile at time $t = 0.02$.

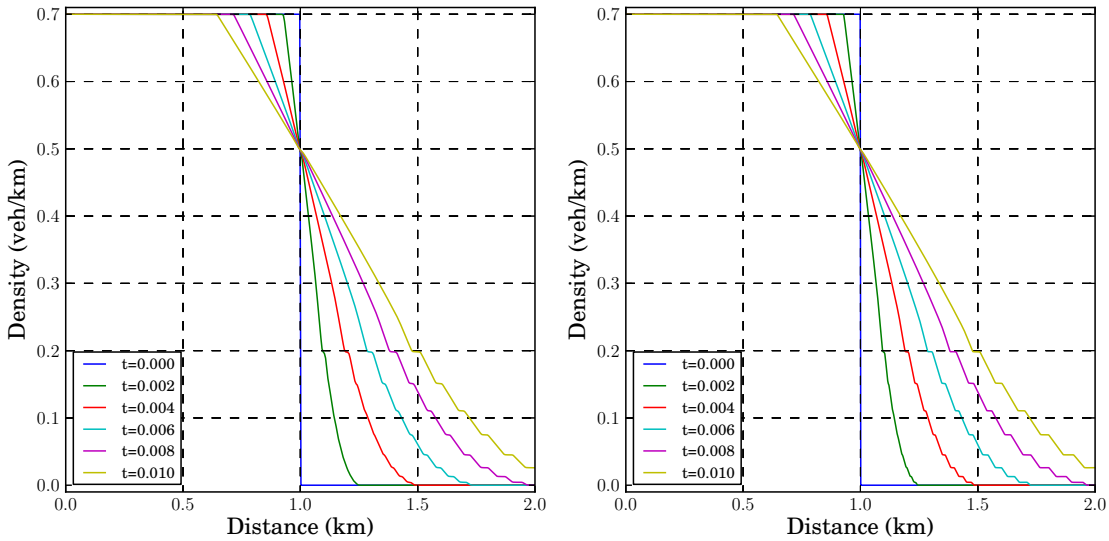

(a) $N = 400$ (b) $N = 800$

Figure 5.15: A transonic rarefaction is computed with $N = 400$ and $N = 800$. The sonic point is at $x = 1$ and is clearly smoother in the $N = 800$ grid cell case.

Chapter 6

Conclusions

Our approach to the study of multi-class traffic flow is based on solving a system of hyperbolic PDEs derived from the Lighthill-Whitham and Richards (LWR) model. This extension of the LWR model to incorporate multiple driver types was first proposed by Wong and Wong [25] in 2002 in which each driver class was characterized by its desired maximum velocity. Our focus has been to implement a finite volume method of Godunov-type that makes use of an approximate Riemann solver. We compare our results to other published work in the literature [25, 28, 29] for systems with up to nine classes of drivers.

We begin by deriving the exact solution to the Riemann problem for the case with two driver classes. This requires an understanding of the Hugoniot locus for shocks and integral curves for smooth solutions that describe the solution path joining arbitrary left and right states. An understanding of these curves reveals that the two elementary waves emanating from the initial discontinuity are determined by the location of the right state relative to the Hugoniot loci and integral curves through the left state. In particular, the constant middle state is determined by the intersection of the 1-curve through the left state and the 2-curve through the right state.

This analysis motivates our use of a Godunov-type method that incorporates a local Riemann solver. Our experience in deriving the exact solution to the Riemann problem for the two-class case suggests that using an exact Riemann solver in the numerical scheme would be too expensive. Therefore, we use an approximate Riemann solver of Roe type instead.

An approximate Riemann solver of Roe type requires a linearized Roe matrix that we derive for a general number of driver classes. We then determine an entropy fix so that

the numerical solution is consistent for transonic rarefaction waves. The algorithm is implemented in Fortran using the CLAWPACK software package [16].

A convergence study shows that our method is first order accurate in space. We then compare to several different studies in the literature with three and nine classes of drivers. In the three-class study we find that our method shows better resolution of the middle states where the comparison case shows small oscillations using a fifth order WENO method. In the nine-class study, we obtained similar accuracy to other published results. While we cannot draw conclusions about which scheme is better suited for this problem, we can say that incorporating knowledge of the solution to the Riemann problem into the finite volume scheme yields results with similar accuracy to the WENO scheme even when half the number of grid cells are used.

Appendix

1-wave, 2-wave

For $\lambda_1 < \lambda_2$ we claim that the 1-wave which connects $\vec{q}_L$ to $\vec{q}_M$ is determined only by the relative size of $\lambda_1(\vec{q}_L)$ and $\lambda_1(\vec{q}_M)$ while the 2-wave which connects $\vec{q}_M$ to $\vec{q}_R$ is determined only by the relative size of $\lambda_2(\vec{q}_M)$ and $\lambda_2(\vec{q}_R)$.

Shock-Shock Case

Given that both the 1-wave and 2-wave are shocks, with s_L being the left most shock and s_R the right most shock, the above statement suggests that

$$\lambda_1(\vec{q}_L) > s_L > \lambda_1(\vec{q}_M) \tag{6.1}$$

and

$$\lambda_2(\vec{q}_M) > s_R > \lambda_2(\vec{q}_R) \tag{6.2}$$

must hold by the Lax-entropy condition.

Now let's assume the opposite is true. Let the 1-wave be defined by the λ_2 characteristics and the 2-wave by the λ_1 characteristics. Then the lax entropy condition says that

$$\lambda_2(\vec{q}_L) > s_L > \lambda_2(\vec{q}_M) \tag{6.3}$$

and

$$\lambda_1(\vec{q}_M) > s_R > \lambda_1(\vec{q}_R) \tag{6.4}$$

must hold. But this leads to a contradiction. Since $\lambda_1(\vec{q}_M) < \lambda_2(\vec{q}_M)$ by assumption it follows that $s_R < s_L$. In other words, the right most shock is to the left of the left most shock.

Rarefaction-Rarefaction Case

Given that both the 1-wave and 2-wave are rarefactions the above statement suggests that

$$\lambda_1(\vec{q}_L) < \lambda_1(\vec{q}_M) \tag{6.5}$$

and

$$\lambda_2(\vec{q}_M) < \lambda_2(\vec{q}_R) \tag{6.6}$$

must hold.

Again let's assume the opposite is true. Let the 1-wave be defined by the λ_2 characteristics and the 2-wave by the λ_1 characteristics. Then

$$\lambda_2(\vec{q}_L) < \lambda_2(\vec{q}_M) \tag{6.7}$$

and

$$\lambda_1(\vec{q}_M) < \lambda_1(\vec{q}_R) \tag{6.8}$$

must hold. This leads to an immediate violation of the assumption that $\lambda_1(\vec{q}_M) < \lambda_2(\vec{q}_M)$.

Bibliography

[1] Saad A. H. Algadhi and Hani S. Mahmassani. Simulation of crowd behavior and movement: Fundamental relations and application. *Transportation Research Record*, 1320:260–268, 1991.

[2] P. Bagnerini and M. Rascle. A multiclass homogenized hyperbolic model of traffic flow. *SIAM J. Math. Anal.*, 35:949–973, 2003.

[3] Sylvie Benzoni-Gavage and Rinaldo M. Colombo. An n-populations model for traffic flow. *European Journal of Applied Mathematics*, 14:587–612, 2003.

[4] Hsun-Jung Cho and Shih-Ching Lo. Modeling self-consistent multi-class dynamic traffic flow. *Physica A*, 312:342–362, 2002.

[5] Richard R. Clements and Roger L. Hughes. Mathematical modelling of a mediaeval battle: The battle of Agincourt, 1415. *Mathematics and Computers in Simulation*, 64:259–269, 2004.

[6] R. M. Colombo. A 2 x 2 hyperbolic traffic flow model. *Mathematical and Computer Modelling*, 35:683–688, 2002.

[7] Carlos F. Daganzo. A continuum theory of traffic dynamics for freeways with special lanes. *Transportation Research B*, 31:83–102, 1996.

[8] Rosa Donat and Pep Mulet. Characteristic-based schemes for mulit-class Lighthill-Whitham-Richards traffic models. *Journal of Scientific Computing*, 37:233–250, 2008.

[9] A. K. Gupta and V. K. Datiyar. A new multi-class continuum model for traffic flow. *Transportmetrica*, 3:73–85, 2007.

[10] M. Herty, C. Kirchner, and S. Moutari. Multi-class traffic models on road networks. *Communications in Mathematical Sciences*, 3:591–608, 2006.

[11] M. H. Holmes. *Introduction to the Foundations of Applied Mathematics*. Springer, 2009.

[12] Serge P. Hoogendoorn and Piet H. L. Bovy. Continuum modeling of multiclass traffic flow. *Transportation Research Part B: Methodological*, 34:123–146, 2000.

[13] Serge Paul Hoogendoorn. *Multiclass continuum modelling of multilane traffic flow*. PhD thesis, Delft University of Technology, 1999.

[14] J. P. Lebacque. The godunov scheme and what it means for first order traffic flow models. In J. B. Lesort, editor, *Transportation and Traffic Theory: Proceedings of the 13th International Symposium on Transportation and Traffic Theory, Lyon, France*, pages 647–677, 1996.

[15] Randall J. LeVeque. *Numerical Methods for Conservation Laws*. Birkhauser Verlag, second edition, 1992.

[16] Randall J. LeVeque. *Finite Volume Methods for Hyperbolic Problems*. Cambridge University Press, 2002.

[17] M. J. Lighthill and G. B. Whitham. On kinematic waves: II a theory of traffic flow on long crowded roads. In *Proceedings of the Royal Society, London, Series A*, volume 229, pages 217–345, 1955.

[18] Tai-Ping Liu. The Riemann problem for general 2 x 2 conservation laws. *Transactions of the Amer. Math Soc.*, 199:89–112, 1974.

[19] S. Logghe and L. H. Immers. Multi-class kinematic wave theory of traffic flow. *Transportation Research B*, 42:523–541, 2008.

[20] P. I. Richards. Shock waves on the highway. *Operations Research*, 4:41–51, 1956.

[21] Al-Nasur J. Sadeq. *New Models for Crowd Dynamics and Control*. PhD thesis, Virginia Polytechnic Institute, Blacksburg, 2006.

[22] Chi-Wang Shu. Essentially non-oscillatory and weighted essentialy non-oscillatory schemes for hyperbolic conservation laws. ICASE Report 97–65, NASA Langley Research Center, Langley, VA, 1997.

[23] Huazhong Tang. On the sonic point glitch. *Journal of Computational Physics*, 202:507–532, 2005.

[24] E. F. Toro. *Riemann Solvers and Numerical Methods for Fluid Dynamics*. Springer, second edition, 1999.

[25] G. C. K. Wong and S. C. Wong. A multi-class traffic flow model - an extension of LWR model with heterogeneous drivers. *Transportation Research A*, 36:827–841, 2002.

[26] Zhimin Xie, Zuojin Zhu, and JunJian Hu. Numerical study of mixed freeway traffic flows. *Communications in Numerical Methods in Engineering*, 22:33–39, 2006.

[27] H. M. Zhang and W. L. Jin. A kinematic wave traffic flow model for mixed traffic.

[28] Mengping Zhang, Chi-Wang Shu, George C. K. Wong, and S. C. Wong. A weighted essentially non-oscillatory numerical scheme for a multi-class Lighthill-Whitham-Richards traffic flow model. *Journal of Computational Physics*, 191:639–659, 2003.

[29] Peng Zhang, Ru-Xun Liu, S. C. Wong, and Shi-Qiang Dai. Hyperbolicity and kinematic waves of a class of multi-population partial differential equations. *European Journal of Applied Mathematics*, 17(2):171–200, 2006.

[30] Peng Zhang, S. C. Wong, and Chi-Wang Shu. A weighted essentially non-oscillatory numerical scheme for a multi-class traffic flow model on an inhomogeneous highway. *Journal of Computational Physics*, 212:739–756, 2006.

[31] Peng Zhang, S. C. Wong, and Zhenli Xu. A hybrid scheme for solving a multi-class traffic flow model with complex wave breaking. *Computer Methods in Applied Mechanics and Engineering*, 197:3816–3827, 2008.